DOKUZ EYLÜL UNIVERSITY

GRADUATE SCHOOL OF NATURAL AND APPLIED SCIENCES

IMPACT CHARACTERISTICS OF LAMINATED COMPOSITES

by

Eray SABANCI

August, 2012

İZMİR

IMPACT CHARACTERISTICS OF LAMINATED COMPOSITES

A Thesis Submitted to the
Graduate School and Applied Sciences of Dokuz Eylül University
In Partial Fulfillment of the Requirements for the
Degree of Master of Science in
Mechanical Engineering, Mechanics Program

by
Eray SABANCI

August, 2012
İZMİR

We have read the thesis entitled **"IMPACT CHARACTERISTICS OF LAMINATED COMPOSITES"** completed by **ERAY SABANCI** under supervision of **PROF. DR. RAMAZAN KARAKUZU** and we certify that in our opinion it is fully adequate, in scope and in quality, as a thesis for the degree of Master of Science.

Prof. Dr. Ramazan KARAKUZU

Supervisor

Assoc. Prof. Dr. B. Murat İÇTEN

(Jury Member)

Assist. Prof. Dr. Bahadır UYULGAN

(Jury Member)

Prof. Dr. Mustafa SABUNCU

Director

Graduate School of Natural and Applied Sciences

ACKNOWLEDGEMENTS

IMPACT CHARACTERISTICS OF LAMINATED COMPOSITES

ABSTRACT

In this study, the influence of size and location of embedded delamination on impact behavior of laminated composite is investigated, experimentally. The fiber-reinforced composite materials used in this study was manufactured at Composite Laboratory in Dokuz Eylül University, and was prepared by cutting defined size for tests in Izoreel Firm, and they consist of 12 plies lamine is designed as defined orientation.

The specimens were produced as for with and without delamination by vacuum assisted resin infusion molding method (VARIM). As matrix materials, the mixture of Durateks DT E 1000 epoxy and Durateks DT S 1105 hardener resin; and as reinforcement materials, unidirectional E-glass fabric were used. The experiments were performed by using Ceast-Fractovis Plus impact test machine. As a result of the experiments, the location of delamination on the impact behavior is seen to be more effective than the size of delamination.

Keywords: Laminated composites, embedded delamination, impact behavior

TABAKALI KOMPOZİTLERİN DARBE KARAKTERİSTİKLERİ

ÖZ

Bu çalışmada, gömülü delaminasyonların boyut ve konumunun tabakalı kompozitlerin darbe davranışları üzerine etkisi deneysel olarak incelenmiştir. Bu çalışmada kullanılan fiber takviyeli kompozit malzeme Dokuz Eylül Üniversitesinde ki kompozit laboratuarında üretilmiştir ve testler için belirlenen boyutlardaki numuneler İzoreel firmasında kesilerek hazırlanmıştır. Numuneler belirlenen oryantasyon açısında 12 tabakanın birleşimi olarak tasarlandı.

Test numuneleri delaminasyonsuz ve delaminasyonlu olarak vakum destekli reçine infüzyon kalıplama yöntemi kullanılarak üretildi. Matriks malzemesi olarak; Durateks DT E 1000 epoksi and Durateks DT S 1105 sertleştirici reçine karışımı, takviye malzemesi olarakta; tek yönlü E-cam kumaş kullanıldı. Deneyler Ceast-Fractovis Plus test cihazı kullanılarak yapılmıştır. Sonuç olarak, delaminasyon konumunun delaminasyon boyutuna göre darbe davranışları üzerinde daha etkili olduğu görülmüştür.

Anahtar sözcükler: Tabakalı kompozitler, gömülü delaminasyon, darbe davranışı

CONTENTS

CHAPTER ONE
INTRODUCTION

In recent years, composite materials have been widely used in almost all engineering fields such as automotive, aerospace, civil engineering structures, due to their higher stiffness/weight and strength/weight ratios compared to traditional metallic materials, replacing not only steel, light alloys in the construction of some parts of vehicular body, spacecraft, and aerodynamic structures, etc. as well.

Composite materials are exposed to a broad spectrum of loadings during in-service use. Dynamic impact loadings, especially in many cases of impact, require a serious design condition for using of laminated composites for in-service applications. For instance, during the manufacturing process or maintenance, tools can be dropped on the structure of the aforenamed industries. In this case, although impact velocities are small, the influence of the mass is larger. One of the properties of the laminated composite structures is more susceptible to impact damage than similar metallic structures. If a composite laminate is subjected to low-velocity impact, invisible damage consisting of internal delamination might be occurred. This internal damage can cause severe reductions in strength and can grow under load. Because of an effective design of composite structures, it becomes very significant to understand the impact induced damage mechanisms in laminates. Due to these reasons, numerous experimental and analytical techniques have been developed to study the dynamic response of the composite structures in the dynamic loading phenomenon.

Many investigations have been carried out which related to the impact on composite structures. (Hosur, Adbullah & Jeelani, 2005) studied to determine the response of four different combinations of hybrid laminates subjected to low velocity impact loading, experimentally. To compare the response of hybrid laminates, they also investigated carbon/epoxy and glass/epoxy laminates. They used twill weave carbon fabric and plain weave S2-glass fabric using vacuum assisted resin molding process with SC-15 epoxy resin system. Effect of permanent indentation on the

delamination threshold for small mass impacts on composite structures which caused by hailstones and runway debris was carried out by (Zheng & Binienda, 2007). They used an elastic-plastic contact law which accounts for permanent indentation and damage effects to study small mass impact on laminated composite plates. Compared to the results obtained using the Hertzian contact law, it was found that damage can change the dynamic response of the structure significantly with increasing impact velocity. They obtained good agreement between the predicted threshold values and published experimental results. The characterization of high and low speed impact damage in carbon fiber reinforced plastics was investigated by (Symons, 2000). Results show that the delamination areas of high and low speed impact are similar for the same impact energy and so the permanent indentation is greater for high speed impact. (Aktas, Atas, Icten & Karakuzu, 2009) and (Icten, Atas, Aktas & Karakuzu, 2009) studied the impact response of unidirectional glass/epoxy laminates in room and low temperature conditions by considering energy profile diagrams and associated load–deflection curves.

(Sadasivam & Mallick, 2002) carried out the low energy impact characteristics of four different E-glass fibers reinforced thermoplastic and thermosetting matrix composites. Besides, they determined the residual tensile strength of the impact damaged composites, as a function of the input impact energy. The low velocity impact tests on carbon/epoxy laminates of different thicknesses were made by (Caprino, Lopresto, Scarponi & Briotti, 1999). The force and absorbed energy at the onset of delamination, the maximum force and related energy, and penetration energy were evaluated in their study. (Datta, Krishna & Rao, 2004) examined the effects of variable impact energy and laminate thickness on the low velocity impact damage tolerance of GFRP composite laminates. Additionally, they determined critical values of impact energy and laminate thickness. An experimental study to understand the effects of reinforcement geometry on damage progress in woven composite panels under repeated impact loading were presented by (Baucom & Zikry, 2005). (Fuoss, Straznicky & Poon, 1998a, 1998b) investigated the effects of key stacking sequence parameters on the impact damage resistance in composite laminates.

(Mitrevski, Marshall, Thomson, Jones & Whittingham, 2005) and (Mitrevski, Marshall & Thomson, 2006) studied to investigate the effect of impactor shape on the impact response of composite laminates using a drop weight test rig. (Whittingham, Marshall, Mitrevski & Jones, 2004) presented a very useful work related to the effect of an initial pre-stress on the response of carbon–fiber/epoxy laminated plates subjected to low velocity impact. Prior to impact event, they used the specimens which loaded either uniaxially or biaxially by using a specially designed test rig. The impact behavior and post impact compressive characteristics of glass carbon hybrid composites with alternative stacking sequences were investigated by (Naik, Ramasimha, Arya, Prabhu & Shamarao, 2001). They have concluded that hybrid composites are fewer notches sensitive as compared to only carbon or only glass composites. (Atas & Liu, 2008) presented an investigation for the impact response of woven composites with small weaving angles. They determined a method for preparing novel woven composites with small weaving angles. Besides, they examined the effects of the weaving angle on impact characteristics such as peak force, contact duration, maximum deflection and absorbed energy. The influence of velocity in low velocity impact testing of woven and nonwoven composites was carried out by (Rydin, Bushman & Karbhari, 1995). They also obtained that impact velocity only affects the initial part of load curve. In addition to these, the peak force is essentially a function of impact energy and increases linearly with the impact energy up to the point when penetration starts. (Belingardi & Vadori, 2002) carried out the low velocity impact tests of the laminated glass-fiber/epoxy matrix composite plates. They used unidirectional and woven glass fabrics as reinforcing material, and epoxy as matrix. Test specimens which have three different stacking sequences were used in their study.

(Evci & Gülgec, 2012) presented an experimental investigation to examine the material behavior and low velocity impact performance of fiber reinforced composites depend on several factors such as material properties of reinforcement, fabric structure, mechanical properties of matrix, number and order of layers in composite structure and projectile velocity.

(Akin & Senel, 2010) presented an experimental study to determine the response of E-glass/epoxy laminated plates subjected to low velocity impact loading. Impact tests were performed using a specially designed vertical drop-weight testing machine. The specimens were produced as 8 plies symmetric laminated composites. The specimens stacking sequences were selected as $[0^°/90^°]_{2s}$, $[-30^°/30^°]_{2s}$, $[-45^°/45^°]_{2s}$, and they were compared with each other. Specimens were impacted at constant weight and different impact energies. The studies were carried out on plate dimension of 140×140 mm with both four and two opposite sides clamped. Results show that clamping the material at its four sides makes more stable structure compared to two side clamping.

(Uyaner & Kara, 2007) studied to examine the dynamic response of E-glass/epoxy composite laminates under low velocity impact, experimentally. They used unidirectional reinforced E-glass/epoxy laminates with the stacking sequence of $[0^°/-45^°/45^°/0^°/90^°/0^°/45^°/-45^°/0^°]_s$. They selected the impactor mass as 30 kg for three different impact velocities (2.0, 2.5, and 3.0 m/s). The impact tests were performed by developing special vertical drop weight testing machine. The radius of the impactor with a semispherical nose was 12 mm. The dimensions of specimens were selected as 180×50 mm, 180×100 mm, and 180×150 mm. Besides, the samples were clamped from two opposite sides while the other sides were free. The impact loading were applied the center of each plate. They also characterized the differences in the impact responses of specimens with width. Additionally, results showed that the peak force increased as the increase of the width of the specimen.

A numerical study carried out by (Freitas, Silva & Reis, 2000) to examine the failure mechanism in composite specimens subjected to impact loading. Results show that the numerical evaluation of impact with a linear static finite element analysis is not very accurate, but it gives a meaningful insight on the major mechanisms of failure. (Zhang, Zhu & Lai, 2006) made series of finite element analyses to predict damage initiation and propagation in laminated carbon/epoxy composite plates subjected to low-velocity impact by using ABAQUS commercial software. The delamination threshold load for small mass/high velocity impact on

transversely isotropic plates with different thicknesses by using LS-DYNA finite element software was investigated by (Olsson, Donadon & Falzon, 2006). The damage prediction in composite plates subjected to low-velocity impact by using the finite element analysis was carried out by (Tiberkak, Bachene, Rechak & Necib, 2008). Results showed that the increase of the 90° plies causes the increase in the contact force and a reduction in the rigidity of laminate. (Cho & Zhao, 2002) presented the influence of geometric and material parameters such as span to stiffness ratio, out-of-plane stiffness, stacking sequence on mechanical response of graphite epoxy composites under low velocity impact. They carried out their study by using both two and three dimensional finite element methods combined with the modified Hertzian contact law. (Chakraborty, 2007) presented a 3D finite element analysis for assessing delamination at the interfaces of graphite/epoxy laminated fiber reinforced plastic composites subjected to low velocity impact of multiple cylindrical impactors. Eight nodded layered solid elements were used for the finite element analysis of fiber reinforced plastic laminates. Newmark-b method along with Hertzian contact law was used for transient dynamic finite element analysis and an algorithm was developed to determine the response of the laminated plate under the multiple impacts at different time. The location and extent of delamination due to multiple impacts were assessed by using appropriate delamination criterion. He also carried out a study to observe the effects of important parameters on the impact response of the laminate and the delamination induced at the interfaces. Results showed that both the contact force magnitude and delamination at the interface were extremely influenced by the time interval between successive multiple impacts.

Some of the experimental and numerical studies which carried out in this field are; (Karakuzu, Erbil & Aktas, 2010) presented both experimental and numerical analysis to investigate some parameters such as the effects of impact energy, impactor mass and impact velocity on the maximum contact force, maximum deflection, contact time, absorbed energy, and overall damage area of glass/epoxy laminated composites. The impact event has been simulated and analyzed by using 3DIMPACT finite element code.

The impact behavior of glass/epoxy laminated composite plates under low velocity impact was investigated by (Mili & Necib, 2001), theoretically and experimentally. The experiment material consisted of unidirectional E-glass fiber and epoxy resin. Their thickness was selected 1.8 mm. These plates were cut by means of water jet to obtain three symmetric cross-ply laminated specimens having a circular form and which are $[0^{\circ}_2/90^{\circ}_6/0^{\circ}_2]$, $[0^{\circ}_3/90^{\circ}_4/0^{\circ}_3]$, and $[0^{\circ}_4/90^{\circ}_2/0^{\circ}_4]$. They only presented the force–time histories in their paper. (Tita, Carvalho & Vandepitte, 2008) studied experimentally and numerically to analyses the stacking sequence and impact energy effect on thin carbon/epoxy laminated composite plates under low-velocity impact. (Li, Hu, Cheng, Fukunaga & Sekine, 2002) presented an experimental and numerical investigation on low-velocity impact-induced damage of continuous fiber- reinforced composite laminates. (Wu & Chang, 1989) examined a transient dynamic finite element analysis for studying the response of laminated composite plates exposed to transverse impact loading by a foreign object. They determined some parameters and distribution during the impact event, such as displacements, the transient stress and the strain distributions through the thickness of the laminate.

(Aslan, Karakuzu & Okutan, 2003) and (Aslan, Karakuzu & Sayman, 2002) studied to examine the effects of the impactor velocity, thickness and in-plane dimensions of target and impactor mass on the response of laminated composite plates under low velocity impact, numerically and experimentally. They reached the conclusion that the peak force in an impact event increases with the thickness of the composite as the contact time decreases. A method called the energy profiling method was presented to characterize some impact properties by (Liu, 2004), for instance, penetration and perforation thresholds. The damage modes of impacted composites can also be correlated with the impact properties.

In this study, the influence of size and location of embedded delamination on impact behavior of laminated composite was investigated, experimentally. The fiber-reinforced composite materials used in this study was manufactured Izoreel Firm in Izmir and they consist of 12 plies lamine is designed as defined orientation. The size of test specimens is 100×100 mm, and its stacking sequence is

$[0^{\circ}/90^{\circ}]_6$. The specimens were produced as for with and without delamination by vacuum assisted resin infusion molding method (VARIM). As matrix materials, the mixture of Durateks DT E 1000 epoxy and Durateks DT S 1105 hardener resin; and as reinforcement materials, unidirectional E-glass fabric with a weight of 300 g/m^2 were used. The diameters of delamination were selected as 13 mm, 20 mm and 26 mm; and the impact energies were chosen as 5 J, 10 J, 20 J, 30 J, 40 J and 50 J. Ceast-Fractovis plus impact test machine was used in the experiments. As a result of the experiments, the location of delamination on the impact behavior was seen to be more effective than the size of delamination.

CHAPTER TWO

COMPOSITE MATERIALS

2.1 Engineering Materials

There are so many materials to be found on the commercial market for engineers to design and manufacture products for many engineering applications. These materials range from ordinary materials, which discovered centuries ago, such as copper, iron, e.g., to the more recently developed, advanced materials, composites, ceramics, high-performance steels so on. Due to a broad spectrum of the choice of the materials, the current engineers have a big challenge for the right selection of both materials and manufacturing process for an application. Usages of all of these materials are difficult in the range of these applications; thus, widely classification is necessary for simplification and characterization. These materials can be separated widely from four main categories: (1) metals, (2) plastics, (3) ceramics, and (4) composites with depending on their major characteristics such as stiffness, strength, density, and melting temperature, e.g. (Mazumdar, 2002)

2.1.1 Metals

Metals have been widely used in engineering applications as structural materials for many years. In this field, they have a wide range of design and processing history. Some commonly used metals are iron, aluminum, copper, magnesium, zinc, lead, nickel and titanium. In structural applications, alloys are used more frequently than pure metals. Alloys are formed by mixing different materials, sometimes including nonmetallic elements. Alloys offer better properties than pure metals. For example, cast iron is brittle and easy to corrode, but the addition of less than 1% carbon in iron makes it tougher, and the addition of chromium makes it corrosion resistant. Through the principle of alloying, thousands of new metals are created. Metals are, in general, heavy as compared to plastics and composites. Only aluminum, magnesium, and beryllium provide densities close to plastics. Steel is 4 to 7 times heavier than plastic materials; aluminum is 1.2 to 2 times heavier than

8

plastics. Metals generally require several machining operations to obtain the final product. (Mazumdar, 2002)

2.1.2 Plastics

In the past five years, the productions of plastics, which have been used the most engineering materials over the past decade, they have passed steel production. Plastics are mostly used for automobile parts, aerospace components, and consumer goods because of their light weight, easy usability and corrosion resistance. Plastics are found in the market in the form of sheets, rods, bars, powders, pellets, and granules. With the help of manufacturing process, plastics can be divided into near-net-share or net-share parts. They can obtain high surface finish; therefore, they provide elimination of several machining operations. This feature has advantage of low cost parts. Due to their poor thermal stability, they are not performed on high-temperatures. In general, the operating temperature for plastics is less than 100°C. While some plastics can be used in high temperatures, such as 100°C to 200°C, and their performance don't chance. They can be easily processed because of having lower melting temperatures. (Mazumdar, 2002)

2.1.3 Ceramics

Ceramics, the most rigid of all materials, have strong covalent bonds and provide big thermal stability and high hardness. The major distinguish characteristic of ceramic as compared to metals and they have almost no ductility. Ceramics that have the highest melting point of engineering materials fail in brittle fashion. They make use of for high-temperature and high-wear applications. They are very resistance to most forms of chemical attack. Ceramics cannot be used by common metallurgical techniques and need high-temperature equipment for fabrication. Ceramics are hard to process because of their high hardness; thus, it is necessary to use expensive cutting tools such as cubic boron nitride and diamond tools due to their requiring net-shape forming to final shape. (Mazumdar, 2002)

2.1.4 Composites

Composite materials have been used to solve technological problems for a long time. Introduced in the past five decades, this material attracts attention of industries which is polymeric-based composition. Since then, composite materials have been popular engineering materials and are designed and produced for various application such as automotive components, sporting goods, aerospace parts, consumer goods, in the marine and oil industries. Composite materials have lightweight components and increase awareness regarding product performance, these materials increase usability in global market; on the other hand, and composite materials have started to replace steel and aluminum. Further they provide better performance than other materials. Composite materials replaced steel components can save 60 to 80% in component weight, and 20 to 50% weight by replacing aluminum parts. Due to all of their characteristics, composite materials have been used in the engineering application. (Mazumdar, 2002)

2.2 Definition of Composite Materials

A composite can be defined as a material which is made by combining two or more materials to give a unique combination of properties. In addition to this definition, it can include metals, alloys, plastic co-polymers, minerals and wood. Fiber-reinforced composite materials differ from the aforesaid materials due to their constitutive characteristics that are different as the molecular level to each other and are mechanically separable. In bulk form, the constituent materials work together but remain in their original forms. As a result, we can say that properties of a composite material are better than constituent material properties. Composite materials have been seen for millions of years in nature such as wood, bamboo and bone. The earliest man-made composite materials were consisting of straw and mud to form bricks for building construction. The beginning of this usage is not known exactly, but it is known that Israelites used straw to reinforce mud bricks. Although a little dried mud makes a good strong wall, it is readily break by bending; on the other hand, a little straw is too easy to crumple, but it is hard to stretch. In this context, if

these materials are combined each other they will be form bricks which resist both squeezing and tearing. In here, mud and straw are called "matrix" and "reinforcement" respectively. Plywood which was used by Egyptians, when they realized that wood could be rearranged to achieve superior strength and resistance to thermal expansion as well as to swelling caused by the absorption of moisture, is known another good example of composites. In generally, composite material is formed by reinforcing fibers in a matrix resin. Fibers, particulates or whiskers can be used as the reinforcement materials and the matrix materials can be formed metals, plastics or ceramics. The reinforcements can be made from polymers, ceramics and metals. The fibers can be continuous, long or short. Composites made with a polymer matrix have become more common and are widely used in various industries such as aerospace industry, marine applications and sporting goods industry, etc.

Figure 2.1 A photo for usage of composite material in industrial fields (http://www.populerbilgi.com)

A composite material is consisted by reinforcing plastics with fibers. To develop a good understanding of composite behavior, one should have understanding of what roles of fibers and matrix materials in a composite. Some of them are listed in Table 2.1. (Mazumdar, 2002)

Table 2.1 Roles of the matrix and reinforcements in a composite

Matrix	Reinforcements
❖ Gives shape to the composite ❖ Protects the reinforcements from the environment ❖ Transfers loads to the reinforcements ❖ Contributes to properties that depend upon both the matrix and the reinforcements, such as toughness	❖ Give strength, stiffness, and other mechanical properties to the composite ❖ Dominate other properties such as the coefficient of thermal expansion, conductivity, and thermal transport

One of the reasons which make composites so important is that matrix and reinforcement have complementary nature. However we cannot say all of the properties of composites are advantageous. For each application advantages and disadvantages should be weighed carefully. Some of the advantages and disadvantages of composites are listed in Table 2.2. (Algan, 2009)

Table 2.2 Advantages and disadvantages of composites

Advantages	Disadvantages
❖ Lightweight ❖ High specific stiffness ❖ High specific strength ❖ Tailored properties (anisotropic) ❖ Easily moldable to complex shapes ❖ Part consolidation leading to lower overall system cost ❖ Good fatigue resistance ❖ Crash worthiness ❖ Low thermal expansion	❖ Cost of materials ❖ Lack of well proven design rules ❖ Metal and composite designs are seldom directly interchangeable ❖ Manufacturing difficulties ❖ Fasteners ❖ Low ductility (joints inefficient, stress risers more critical than in metals ❖ Solvent/moisture attack ❖ Damage susceptibility ❖ Hidden damage

2.3 Classification of Composite Materials

Composite materials can be classified according to their matrix materials, reinforcing material structure and their production techniques. There are four generally accepted types of composite materials. These types are listed as follows:

- ❖ Fibrous composite materials that consist of fibers in a matrix
- ❖ Laminated composite materials that consist of layers of various materials
- ❖ Particulate composite materials that are composed of particles in a matrix
- ❖ Combinations of some or all of the first three types

2.3.1 Fibrous Composite Materials

A composite material is a fiber composite if the reinforcement is in the form of fibers. The fibers used can be either continuous or discontinuous in form, for example chopped fibers, short fibers. (Ye, 2003) The main role of the fibers is to carry the loads along their longitudinal directions. Common fiber reinforcing agents may include some materials such as carbon, glass, polyester, etc. Additionally, functions of the matrix are hold fibers together in bulk form and transmit stresses among the reinforcing fibers, also protect the fibers from mechanical and environmental damages. A basic requirement for a matrix material is that its strain at break must be larger than the fibers it is holding.

2.3.2 Laminated Composite Materials

Laminated composite materials are manufactured from layers of at least two different materials which are bonded together (Figure 2.2). Lamination is utilized to combine the best aspects of the constituent layers in order to achieve a more useful material. The ability to structure and orient material layers in a prescribed sequence leads to several particularly significant advantages of composite materials compared with traditionally monolithic materials. The most important their properties are matching the lamina properties and choose the orientations to the prescribed

structural loads. Some properties which can be gained by lamination are strength, stiffness, corrosion resistance, low weight, etc. Laminated composite materials generally consist of unidirectional fiber reinforced laminate. (Ye, 2003)
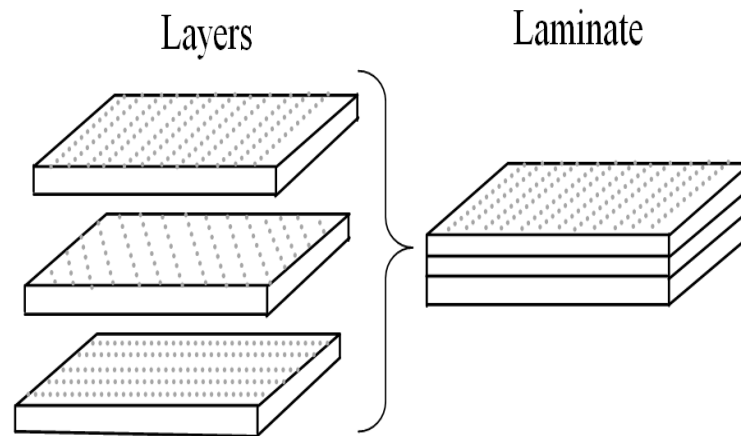

Figure 2.2 A laminate consists of layers with different fiber orientations

2.3.3 Particulate Composite Materials

Particulate composites are produced by using metallic or non-metallic as reinforcing materials in the bulk form. In contrast to fibers, a particle does not have a preferred orientation. Particles are usually utilized to enhance specific properties of materials such as stiffness, temperature behavior, resistance to abrasion, decrease of shrinkage, etc. The load carrying capacity of particle composites depends on the properties of matrix materials. Concrete is a natural example of particle composite. Concrete is made of particles of sand and rock which are bound together by mixture of cement and water. The strength of concrete can be varied by changing the type of matrix materials or using different types of cement.

2.3.4 Combinations of Some or All of the First Three Types

Numerous multiphase composite materials exhibit more than one characteristic of the various classes, fibrous, laminated or particulate composite materials, just discussed. For example, reinforced concrete is both particulate (Since the concrete is

composed of gravel in a cement-paste binder) and fibrous (Owing to the steel reinforcement). Also laminated fiber-reinforced composite materials are obviously both laminated and fibrous composite materials.

Laminated fiber-reinforced composite materials are a hybrid class of composite materials involving both fibrous composite materials and lamination techniques. Here, layers of fiber reinforced material are bonded together with the fiber directions of each layer typically oriented in different direction to give different strengths and stiffness of the laminate in various directions. Thus, the strengths and stiffness of the laminated fiber-reinforced composite material can be tailored to the specific design requirements of the structural element being built. Examples of laminated fiber reinforced composite materials include rocket motor cases, boat hulls, aircraft wing panels and body sections, tennis rackets, golf club shafts, etc. (Jones, 1999)

2.4 Manufacturing Process of Composite Materials

Composite materials are used increasingly in engineering application ranging from aircraft industrials to marina applications instead of traditional materials, because advanced composites have some desirable physical and chemical properties such as high specific stiffness and strength, corrosion resistance, thermal conductivity. According to the end-item design requirements, there are various types of composites processing techniques available to process the various types of reinforcements and resin systems. The test specimens used in this study are manufactured by using vacuum assisted resin infusion molding (VARIM) methods.

2.4.1 Vacuum Assisted Resin Infusion Molding

The vacuum assisted resin infusion molding (VARIM) is one of the manufacturing processes to produce high-quality large-scale components for composite structures. In this process, required number of dry performs reinforcement layers are placed in an open mould and then a plastic vacuum bag is placed on the top of the mould, carefully. The one-sided mould is connected with a resin source

and vacuum pump. The pressure difference between the atmosphere and the vacuum is the driving force for infusion of the resin into the reinforcing fibers. Curing and de-moulding steps follow the impregnation process to finish the product. (Goren & Atas, 2008)

The main steps of the process are:

1. A dry fabric or preform and accompanying materials such as release films, peel plies are placed on tool surface.
2. The preform is sealed with a vacuum bag and the air is evacuated by a vacuum pump.
3. Liquid resin with hardener from an external reservoir is drawn into the component by vacuum.
4. The liquid resin with hardener is infused into the preform until complete impregnation.
5. Curing and de-moulding steps follow the impregnation to finish the product.

The infusion process components used in this work are shown in Figure 2.3. The function of the each component during manufacturing can be summarized as:

- Vacuum bagging films are sealed to the edge of the mould with vacuum bag sealant tape to create a closed system.
- Double side bag sealant tapes are used to provide a vacuum-tight seal between the bag and the tool surface.
- Release films are typically placed directly in contact with the laminate. They separate the laminate from the distribution medium. Release films are often perforated to ensure that any trapped air or volatiles, which may compromise the quality of the laminate, are removed.
- Release fabrics and peel plies are placed against the surface of the laminate. They are woven products which are strong and have good heat resistance. Release films impart a gloss finish on the cured laminate, whereas peel plies

and release fabrics leave an impression of the weave pattern. Peel plies provide a clean, uncontaminated surface for subsequent bonding or painting.

- Tool release materials are used to release the product from tools easily and obtain a smooth surface finish. For this purpose, either self adhesive Teflon films or liquid release agents are utilized. In certain situations Teflon films can also temporarily solve tool porosity problems.

- A highly permeable layer called "resin distribution medium" placed on the top of the preform spreads the resin quickly over the lateral extent of the part.

- Bleeder/breather fabrics are non-woven fabrics allow air and volatiles to be removed from within the vacuum bag throughout the cure cycle. They also absorb excess resin present in some composite lay ups (Goren & Atas, 2008).
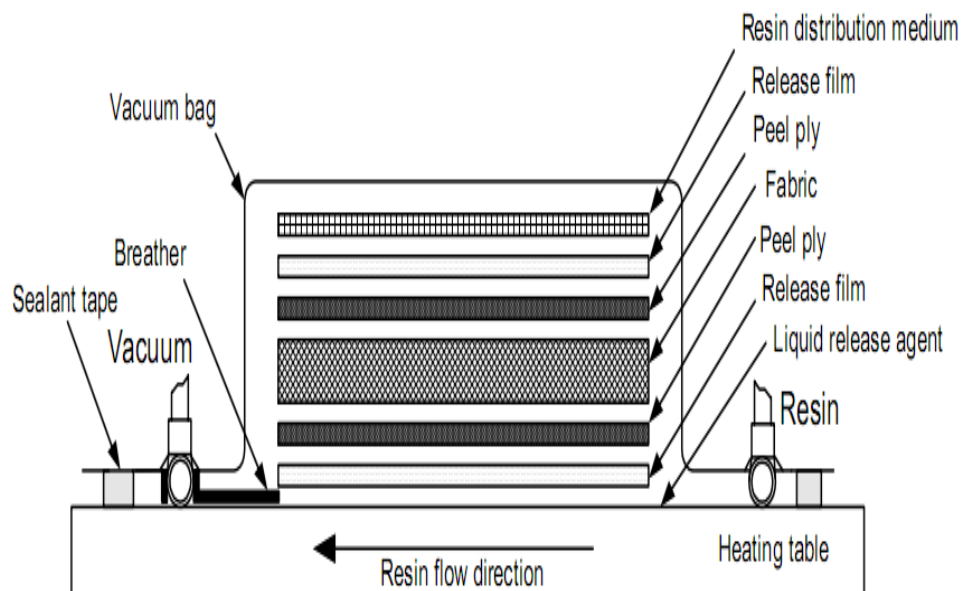
Figure 2.3 Schematic illustration of the vacuum assisted resin infusion molding (VARIM) process (Goren & Atas, 2008)

2.5 Impact on Composite Plates

It is known that composite materials are used more extensively so it may be exposed to various forces, especially during the in-service; they can be exposed to effect of foreign objects impacts. For example, during aircraft take off and landing, debris flying from the runway can cause damage. At this time, projectile has small

mass and high velocity. And another one, any tools which used during the manufacturing or maintenance process can be accidentally dropped on the structure. At this moment, projectile has larger mass and low velocity. (Abrate, 1998) Composite structure is more susceptible to impact damage than similar traditional metallic materials. The result of impact loading may not be directly damage to composite structure. In other words, the composite material which exposed to the impact loading could not be failed, and you will not see any of damage area. But fiber and/or matrix cracks can be occur inside the materials. Many features will be reducing due to this internal damage such as load carrying capacity, and damage can grow under load. In order to understand all of these cases, many researchers have been carried out numerous studies with regard to impact on composite structure during the last decade.

Impact event can be usually classified into three main categories as low velocity, high velocity and hyper velocity impact. However, there is no clear definition to determine the limits of these categories. Some researchers have defined the low velocity impact as up to 10 m/s. Intermediate impact events occurs range from 10 m/s to 50 m/s, and are accepted both low and high velocity impact. Small arms fire or explosive warhead fragments are usually recognized high velocity (Ballistic) impact. Stress wave which is propagation through the thickness of the material dominated high-velocity impact response; thus, the structure does not enough time to respond, leading to a localized damage. Besides, the impact event passes before the stress waves reach the boundary, so boundary condition effects can be ignored. High-velocity impacts range from 50 m/s to 1000 m/s. In hyper velocity impact velocity is also greater than 2-5 km/s, the projectile is moving at very high velocities and the target material behaves like a fluid. (Abrate, 2011)

2.6 Failure Modes

Composite materials can be viewed and analyzed as macroscopic and microscopic viewpoint given in Figure 2.4. In macroscopic viewpoint, the damage modes due to impact can be described four main categories as indentation, penetration, perforation

and bending fracture. Indentation is damage of matrix squash in the impacted area. When penetration took place, the impactor got stuck in the composite plate, and perforation is making a hole into composite plate by impactor nose. The damage surrounding the contact point and the hole is called as respectively penetration and perforation. Bending fractures are generally oblique or transverse, and they may have a butterfly fragment. In microscopic viewpoint, the damage modes can be classified as matrix cracking, delamination and fiber breakage.
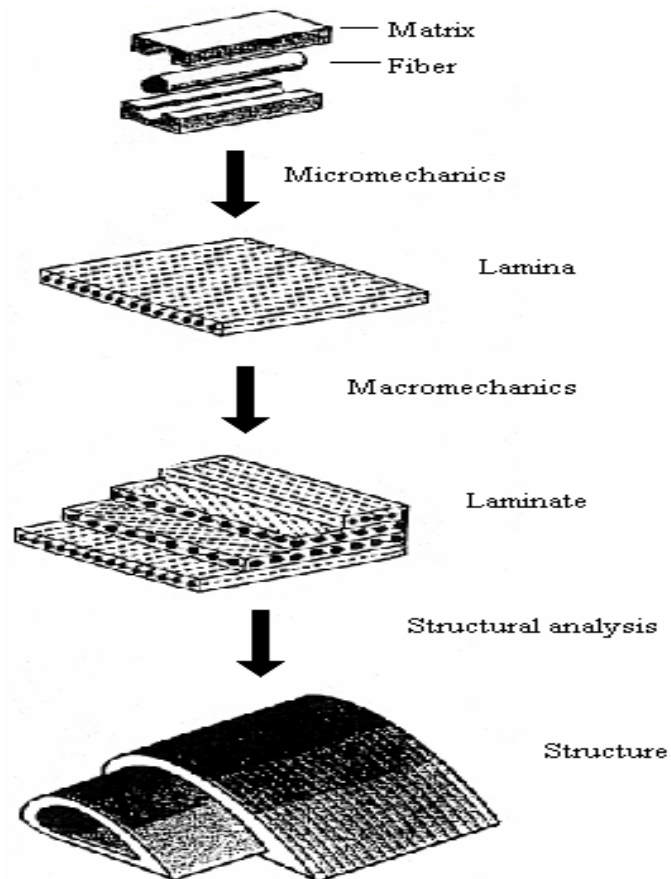
Figure 2.4 Steps of examination and types of analysis for
composite materials (Daniel, 1994)

2.6.1 Matrix Damage

Transverse low velocity impact is caused matrix damage which usually takes the form of matrix cracking, fiber/matrix debonding and delamination initiation. Hardly observable or minimal damage occurs at low impact energy levels (1 to 5 J). Matrix

cracks are usually directed in planes through the fiber direction in unidirectional fiber composites. The matrix damage in the upper layers observes at the contact edges of the impactor. The very high transverse through the material is also caused shear cracks in the middle layers. (Abrate, 2011)

2.6.2 Delamination

Delamination can be identified as debonding between adjacent laminas. They are occurred when the transverse impact energy reaches threshold value, and caused severe reduction of the strength of the laminate. Many experimental studies continually observe that delamination is occurred only interfaces between constituent plies with different fiber orientations. If two adjacent plies have the same fiber orientation, no delamination will be occurred at the interface between them. The delaminated area, which is resulted from point nose impact, usually seems in a peanut or oblong shape for laminated composite with its main axes oriented in the direction of the fibers in the lower ply at that interface.

During the impact event, delamination is initiated from a critical matrix crack, and can grow much more widely thorough the fiber direction than in the transverse direction of the bottom layer at the interface; thus, delamination seems to be in a peanut shape in laminated composites. The delamination shape in laminated composite depending on fiber orientation is illustrated schematically in Figure 2.5. In general, two types of matrix cracks, which then initiate delamination at ply interface, are observed which are called tensile cracks (Bending cracks) and shear cracks as given in Figure 2.6. Tensile cracks initiate when in plane normal stresses exceeded the transverse tensile strength of the ply. Shear cracks are at an angle from the mid-surface which indicates transverse shear stresses play a critical role in their formation. Matrix cracks are firstly observed either in the top layer or in the bottom layer depending on the thickness of the laminate. For thick laminates, matrix cracks are stimulated in the first layer impacted by the impactor because of the high localized contact stresses. Damage progression is in such laminates from the top to down as shown in Figure 2.7.a. In thin laminates, matrix cracks resulting from

bending stresses are in the bottom layer of the laminate and lead to a reversed pine tree pattern shown in Figure 2.7.b.
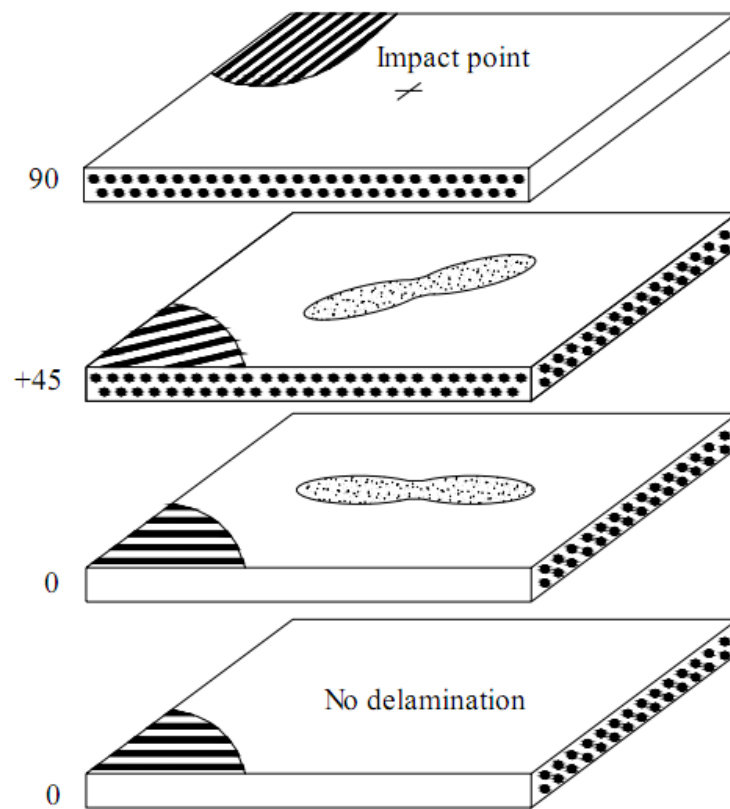

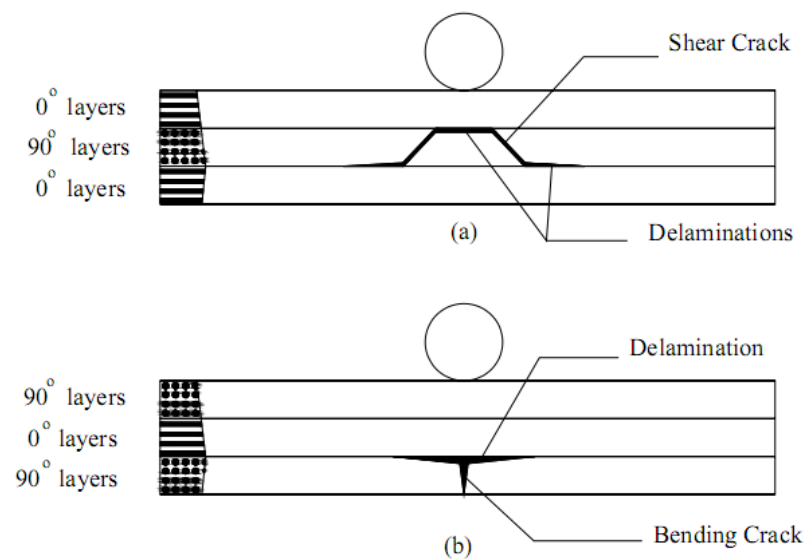Figure 2.5 Delamination shapes in a laminated composite (Abrate, 1998)

Figure 2.6 Delamination initiated by a) inner shear cracks b) a surface bending crack (Abrate, 1998)
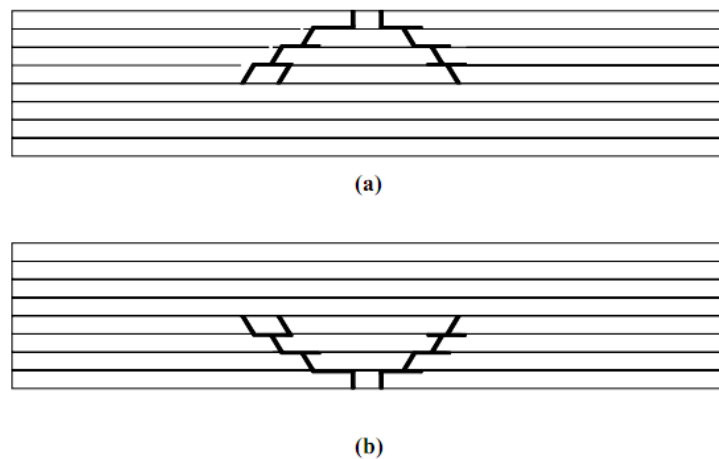
Figure 2.7 Pine tree (a) and reverse pine tree (b) damage patterns
(Abrate, 1998)

2.6.3 Fiber Failure

Fiber failure usually occurs after than the formation of matrix cracking and delamination in the laminate. Fiber failure observes just below the impactor because of the local high stresses and indentation effects which essentially caused by shear forces and on the non-impacted face due to high bending stresses. Fiber failure case is a precursor to catastrophic penetration mode.

2.7 Impact Testing Methods

Impact testing of composites can be carried out by using several types of equipment arrangements. The most typical apparatus for impact studies is the Izod, Charpy impact testers and instrumented falling weight impact testing. During the half part of the 20th century, Izod, who is a metallurgist, researched an impact test for determining the impact test for defining the impact fracture toughness of metal materials. And then Charpy improved this test technique. Until the early 70's, these test methods is widely used in the experimental studies because of providing reliable, qualitative impact data. With the developing strain gage technology, data acquisition, and computers have allowed impact test results to become more quantitative in nature (e.g., force and energy data in digital form).

Several impact techniques have been developed to determine the impact response and damage mechanisms of composite materials. It is very crucial to select an appropriate test method to practice real impact condition. For example, a high velocity impact event, which is required small mass and resulted from a debris flying from the runway to the aircraft component, simulated by using a gas gun. Additionally, a tool which can be dropped on a structure is another example of impact; this event is usually simulated by using a drop weight tester because of requiring larger mass and low velocity.

Ballistic tests are usually performed by using gas gun impact test technique. A projectile pushed by compressed air travels through the gun barrel and passes a speed-sensing device and impacts to the target. A simple speed-sensing device composes of a single light-emitting diode (LED) and a photo detector. Sensor is used to calculate the projectile velocity by the help of the projectile interrupts the light beam and the duration of that interruption in signal.

The specimen is impacted in a direction normal to its surface by using the traditional drop weight impact tests. Heavy impactors are usually guided by a rail during their free fall from a given height. Usually, a sensor activates a device designed to prevent multiple impacts after the impactor bounces back up. The details of drop weight tester and test procedure are given in next chapter. (Icten, 2006)
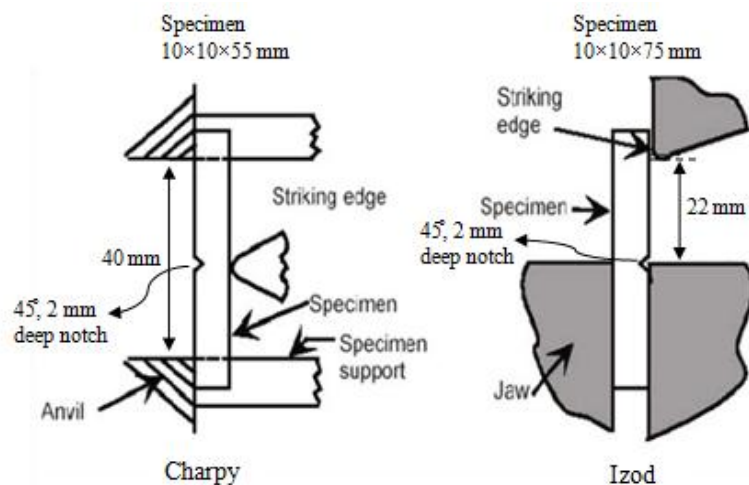
Figure 2.7 Charpy and Izod test configurations for low velocity impact testing (Abrate, 2011)

CHAPTER THREE
EXPERIMENTAL STUDY

3.1 Producing Laminated Composites for Experiment

In this study, the influence of size and location of embedded delamination on impact behavior of laminated composite were investigated, experimentally; therefore, in manufacturing process, delaminations which were defined diameter size as 13 mm, 20 mm and 26 mm by supervisor, created by handle, initially. Delaminations placed in the middle of test specimens are shown in Figure 3.1. Release film was utilized as delamination material because of their specific properties that prevents layers from sticking to each other.

Figure 3.1 Manufacturing process of delamination

The production of composite layers was initiated after the completed the creation process of delamination. In this process, layers size of unidirectional glass fiber laminates were defined as 800×1200 mm, were cut by handle. In addition to this, release film, vacuum bagging film, release fabric and the other component were prepared by cutting handle as appropriate for the dimensions of 800×1200 mm.

Composite laminates which was used to cutting for the specimens manufacturing were produced at Composite Laboratory in the Dokuz Eylül University by using vacuum assisted resin infusion molding (VARIM) methods (Figure 3.2).

Figure 3.2 A photo of vacuum assisted resin infusion molding (VARIM) equipment

Impacted test specimens in this investigation compose of epoxy resin and glass fiber. Additionally, as matrix materials, the mixture of Durateks DT E 1000 epoxy and Durateks DT S 1105 hardener resin; and as reinforcement materials, unidirectional E-glass fabric with a weight of 300 g/m^2 were used. Mass ratios of the mixture of Durateks DT E 1000 epoxy and Durateks DT S 1105 hardener resin were chosen 3/1. The stacking sequence and the size of test specimens were selected as $[0^°/90^°]_6$ and 100×100 mm, respectively. The laminate was planned antisymmetric as identified orientation. Differences between the test specimens are delamination size and location. Namely, delaminations were placed in the different interface from the bottom layer as 2nd, 4th, 6th, $2^{nd}/4^{th}$ and $2^{nd}/4^{th}/6^{th}$ by using a mould. Delaminations were placed in the interface are illustrated in the Figure 3.3. As mould material was utilized the transparent nylons. Appropriate for the laminate dimension which defined 800×1200 mm was cutting by scissor.

And then identified places in which the holes were opened by using a utility knife, and delaminations were inserted onto layers (Figure 3.4). By considered the blade size, the distances of between delaminations were set as 110 mm for the size of specimens were identified as 100×100 mm (Figure 3.4).
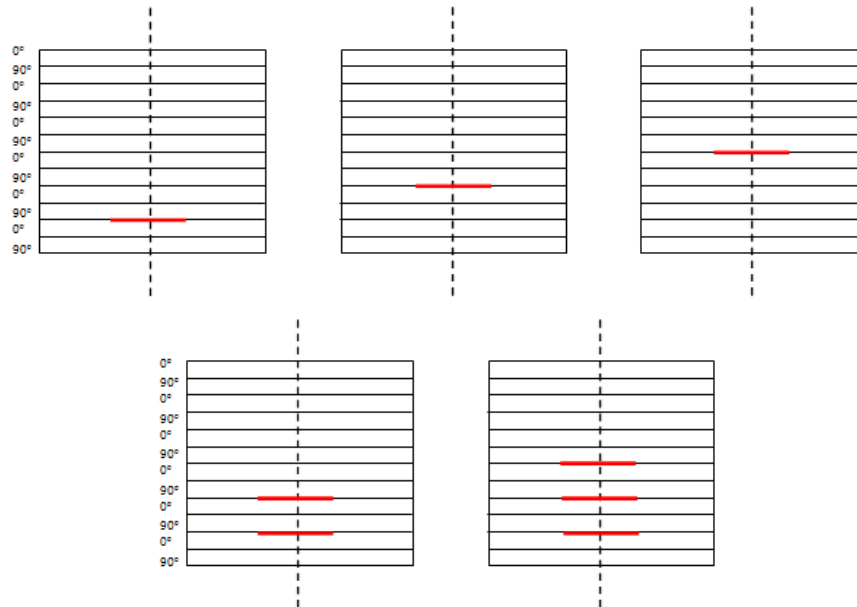
Figure 3.3 A schematic illustrations of the delamination placed in interface
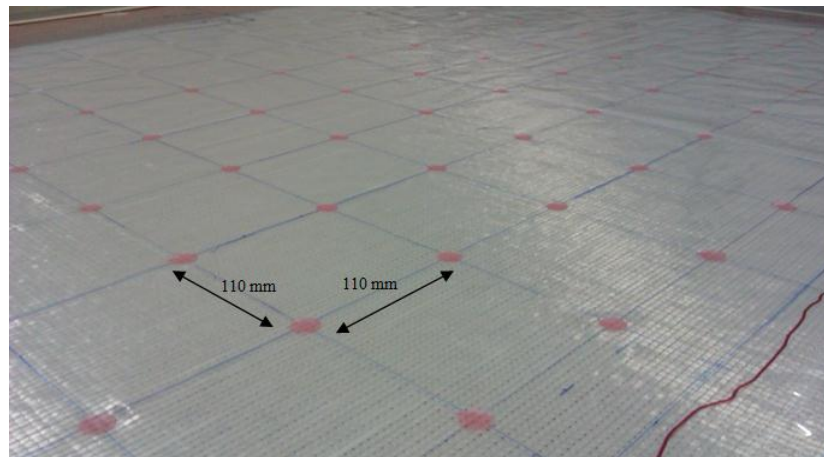
Figure 3.4 A photo of delaminations were placed by using transparent mould

After delaminations were placed onto layer, other layers were overlapping. The others components were already prepared such as release film, vacuum bagging film, release fabric were placed onto the layers. By setting both curing temperature as $90^{\circ}C$ and curing time as 150 min, VARIM equipment was run, and then mixture of epoxy

and resin was impregnated into the mould with the help of vacuum. After completion of all processes, was waited to finish the curing time. When finished the curing time, the laminate was ripped from the VARIM equipment. Finished form of the laminate is shown in Figure 3.5.

Figure 3.5 Finished form of the laminate

In order to produce test specimens, manufactured laminate were cut at Izoreel Firm. Test specimens which made by cutting are shown in Figure 3.6. The numbers of specimens used in the impact tests are given in Table.1.
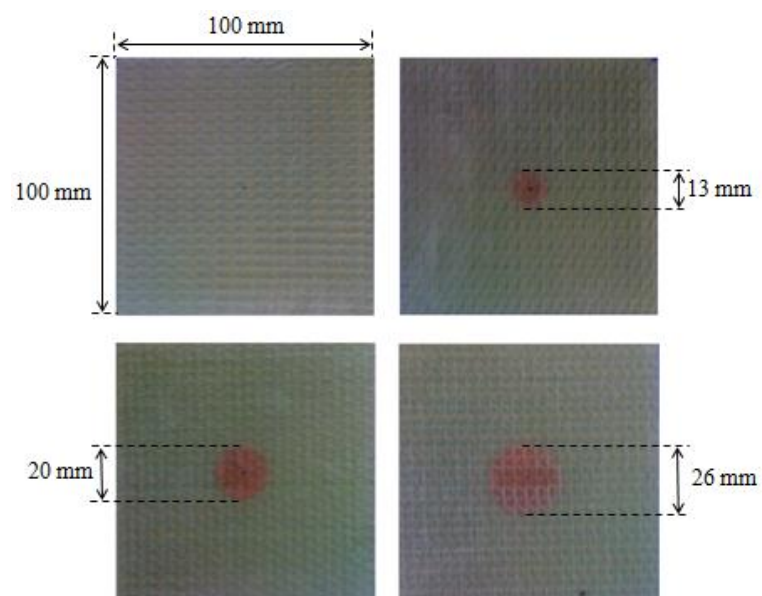
Figure 3.6 A photo of prepared test specimen

Table 3.1 The number of test specimens

The number of interface where placed the delamination.	The diameters of delamination	The number of specimens
No delamination	-	30
2nd	13 mm	30
	20 mm	30
	26 mm	30
4th	13 mm	30
6th	13 mm	30
2nd/4th	13 mm	30
2nd/4th/6th	13 mm	30

The mechanical properties of the specimen were determined as for ASTM testing standards at Composite Laboratory in Dokuz Eylül University. The specimens which used in the experiments were produced the same materials. Mechanical properties of the materials are given in Table 3.2.

Table 3.2 Mechanical properties of the specimens

Longitudinal Modulus	E_1	31400 MPa
Transverse Modulus	E_2	22800 MPa
In-plane Shear Modulus	G_{12}	7500 MPa
Poisson's Ratio	υ_{12}	0.25
Long. Tensile Strength	X_t	677 MPa
Trans. Tensile Strength	Y_t	380 MPa
Long. Comp. Strength	X_c	429 MPa
Trans. Comp. Strength	X_c	211 MPa
In-plane Shear Strength	S_{12}	68 MPa

3.2 Impact Test Machine

The impact tests were performed by using Fractovis Plus impact machine at room temperature, at Composite Laboratory in Dokuz Eylül University (Figure 3.8). The impact energy is incrementally raised from 5 J up to 50 J investigation of the impact energy level. Fractovis Plus impact test equipment is a test machine which can adjust for applications of broad spectrum requiring both low and high impact energies. The impactor, which is a hemispherical steel rod at the end, has a radius of 12.7 mm. The force transducer capacity of test machine is 22.24 kN. The total mass of the impactor, which included crosshead mass and impactor mass, is 5.02 kg. A pneumatic fixture, which is square with 76 mm per edge, was utilized to clamp the specimens (Figure 3.7). To measure the contact force, a load transducer, which located between the cross head and hemispherical tub nose, was utilized. To avoid the repeated impact on the specimens after the impact, an anti-rebounding systems, which located in the test machine, was used. The impactor is rebounded from the specimen surface after the impact event with the help of the excessive energy. The maximum potential energy is up to 1800 J with the additional mass. Besides, to raise the speed of the impactor up to 24 m/s, energy system can be utilized. With the help of data acquisition system (DAS) which allows acquiring 16000 data during tests, the time versus velocity, load, deflection and energy histories were obtained.
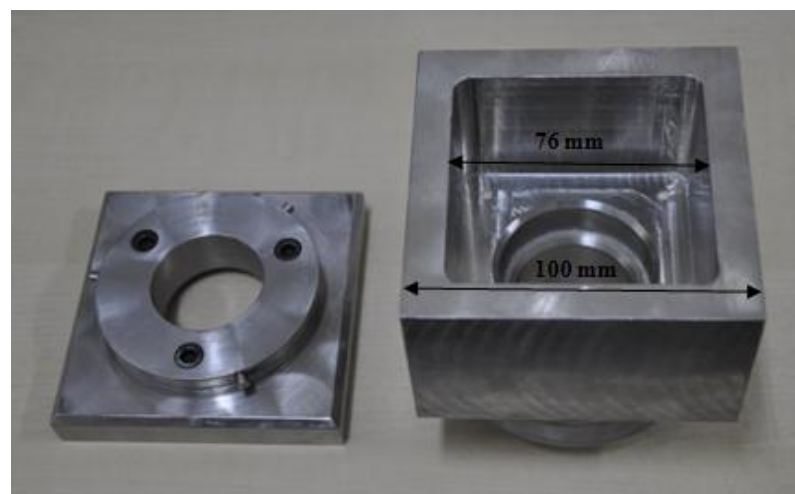
Figure 3.7 A photo of the clamping fixture

Figure 3.7 Fractovis Plus test machine

Fractovis Plus impact test machine and its equipments are listed below:

A : Body of the impact tester

B1: Impactor nose

B2: Piezoelectric impactor nose

C : Data acquisition system (DAS)

D : Specimen holder mechanism

E : Springs

For the same energy levels, five specimens were utilized to investigate the impact characteristics such as force-time, force-deflections curves and absorbed energy. Besides, average values were determined and their relevant graphics, which were given in the next chapter, were drawn.

CHAPTER FOUR
EXPERIMENTAL RESULTS

4.1 Impact Tests

The Fractovis Plus impact test machine is used to perform the impact tests at the Composite Laboratory in Dokuz Eylül University. During the impact tests, the energy is incrementally raised from impact energy level of 5 J up to 50 J. In order to examine the size and location of delamination effects on the impact behavior of glass/epoxy laminated composites, each of the impact tests are carried out by using the specimens which manufactured with and without embedded delamination (13 mm, 20 mm, and 26 mm, etc.) in 2nd interface from the bottom layer (shown as C20d2, etc.), and the same size of embedded delamination as placed in different interface from bottom layer (2nd, 4th, 6th, $2^{nd}/4^{th}$, $2^{nd}/4^{th}/6^{th}$, etc.), which is abbreviated such as C13d2 and C13d2/4/6. Also, specimen which manufactured without delamination is abbreviated as C0d0. The impact test is performed five times for each specimen to select mean value for comment.

The experimental results are grouped under three main categories. The first category is effect of energy levels; the second one is the size of delamination effects on the impact behavior, and the other is the location of delamination effects on the impact behavior. Also, impact response of specimen is detected with the aid of contact force-time and contact force-deflection curves. In this context, the experimental results are given in the subsections.

4.2 Effect of Energy Levels on Impact Behavior

In order to examine effects of delamination size on the impact behavior of laminated composite, the velocity, load, deflection and energy versus time histories are obtained by using the Fractovis Plus test machine with the help of data acquisition system (DAS). The impact energy is selected as 5 J, 10 J, 20 J, 30 J, 40 J and 50 J to clearly see the effects of the size of delamination.

Figure 4.1.a-b represents the contact force-time and the contact force-deflection curve for specimen of C13d2, where abbreviation C13d2 means that diameter of delamination is 13 mm, and embedded delamination is placed in the 2nd interface from the bottom layer, at the all impact energy level.
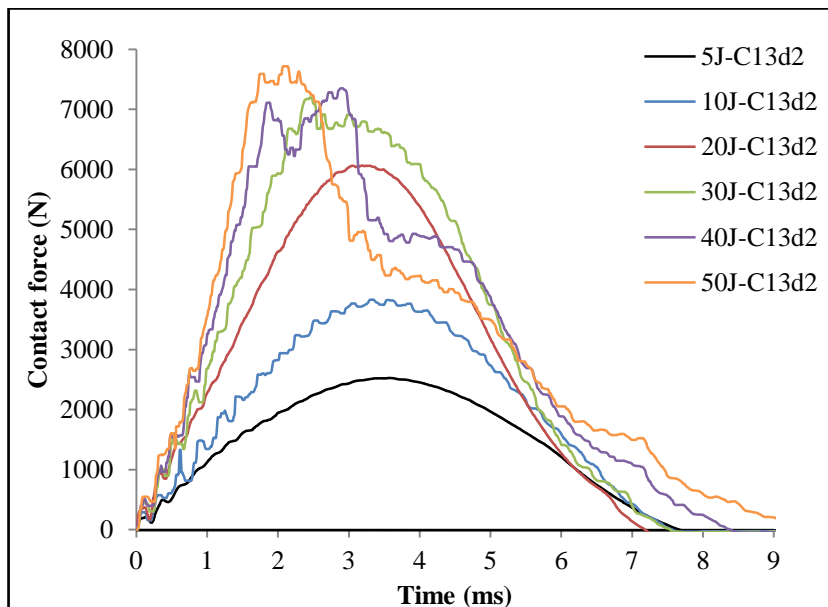
(a)
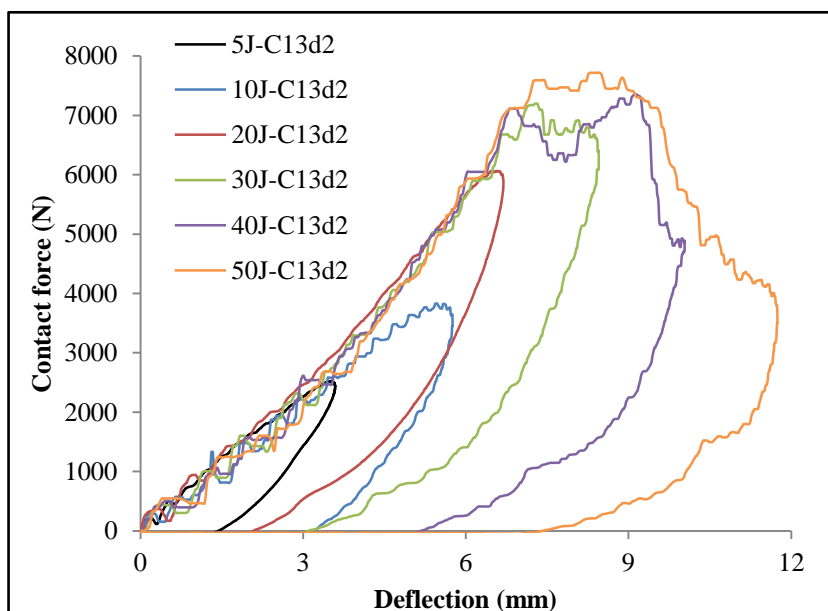
(b)

Figure 4.1 (a) The contact force-time and (b) the contact force-deflection history for specimen of C13d2 at the all energy level

From the Figure 4.1.a-b, it clearly can be said that the contact force is increased by increasing the impact energy level. In addition to this, the impact time increases by increasing impact energy level except for 5 J and 10 J. Also, the deflection curve can express the threshold for the rebounding and penetration case. Rebounding was observed at the all impact energy level. Rebounding can be defined as the impactor rebounded from the specimen after the impact event. And also, penetration can be defined as the impactor sticks into specimen and not reaches the bottom surface of the specimen. For rebounding case, in unloading part, the contact force-time curve needs to be return parallel to the loading part. But, for penetration case, the curve do not return parallel to the loading part.

The contact force is little changed by the increasing energy level among of the 30 J and 50 J. However, when the peak contact force occurred, time is called peak time and changes by the increasing energy level except for 5 J and 10 J. Also, the maximum deflection is obtained at energy level in 50 J. It can be said that the deflection of specimen increases by increasing energy level.

The absorbed energy can be determined from the area under the contact force-deflection curve. The absorbed energy means the total energy that is transferred from the impactor to the specimen. In rebounding case, the amount of energy is returned by the impactor from the specimen depending on the elastic reinstatement. But, for the penetration case, there is no elastic energy returning to impactor. Besides, delamination partly increases with increasing impact energy depending on the absorbed energy.

In loading part, the curves are followed parallel to each other. So, it can be said that the bending stiffness is the same for all case. However, in the unloading part, the curves are shown differs from the each other because of the different damage mechanisms. So, contact time and deflection value changes depending on the different energy levels. There has been observed any significantly effect on impact response of specimen for 5 J and 10 J.

In order to determine the location of delamination effects on the impact behavior of laminated composite, impact tests are performed by using manufactured specimen which has an embedded delamination in the different interface from the bottom layer. The contact force-time and the contact force-deflection curve are drawn by using measured value from the Fractovis Plus test machine with the aid of data acquisition system (DAS). The impact energy is chosen as 20 J, 30 J, 40 J and 50 J to prominently determine the location of delamination effects on the impact response of specimen.

Figure 4.2-5.a-b are given for the showing the curve of the contact force-time and contact force-deflection for specimens of C13d4, C13d6, C13d2/4, and C13d2/4/6 at the all energy level. From these figures, it clearly can be said that the contact force increases depending on the increasing impact energy. As seen in Figure 4.2-5.b, it can be comment that rebounding is occurred at the all impact energy level. For rebounding case, in unloading part, the curve returns parallel to the loading part.

In view of the Figure 4.2-5.a, the maximum contact force value is changed by the increasing impact energy level. Besides, the peak time is changed by the impact energy level. Also, the maximum deflection value is observed as nearly the same for all specimens at the energy level of 50 J. As seen in the Figure 4.2-5.b, the absorbed energy is raised increasing impact energy level; thus, it can be said that damage area rises depending on the absorbed energy.

From result in the Figure 4.2-5.b, in loading part, the curves are followed parallel to each other. According to this, it can be said that the bending stiffness is the same for all case. However, in the unloading part, the curves are shown differs from the each other because of the different damage mechanisms. So, the contact time and deflection value are different depending on the different energy levels. In addition to this, it can be expressed that the location of delamination has an influence on the impact response of specimen.
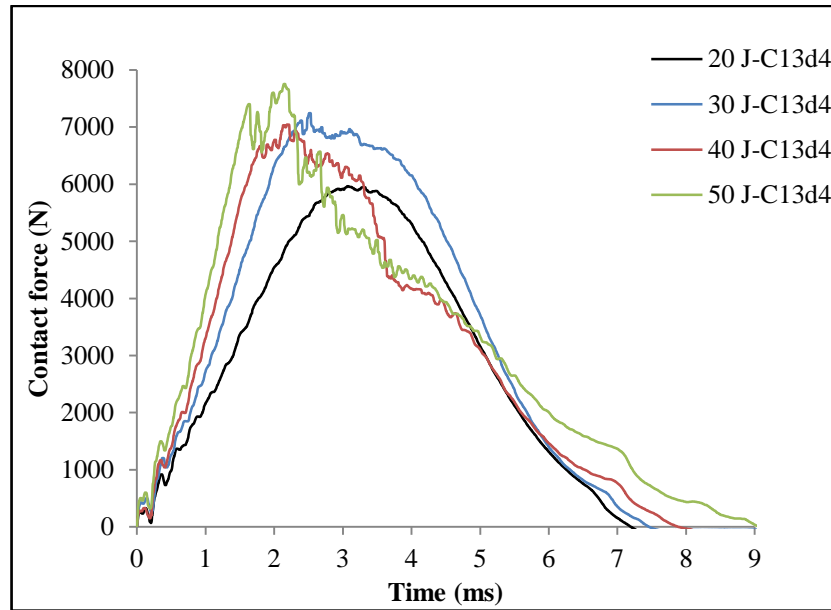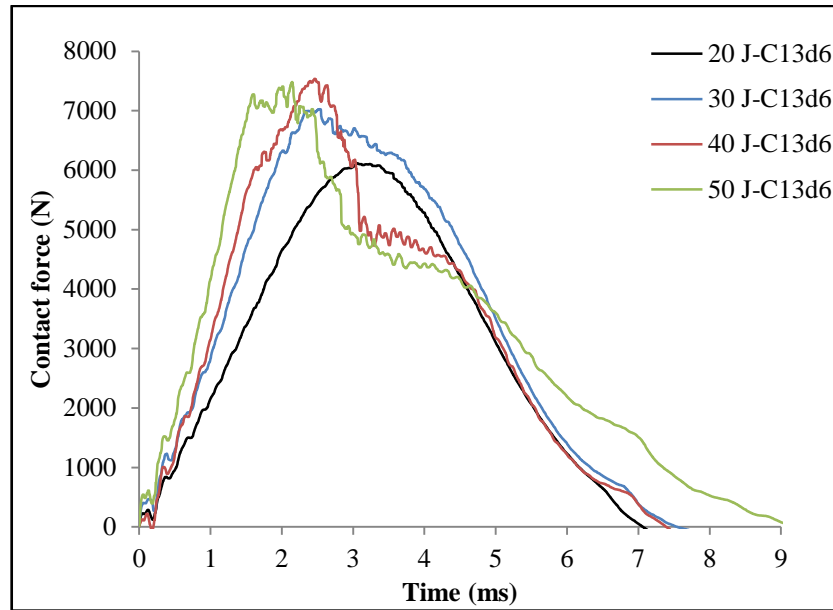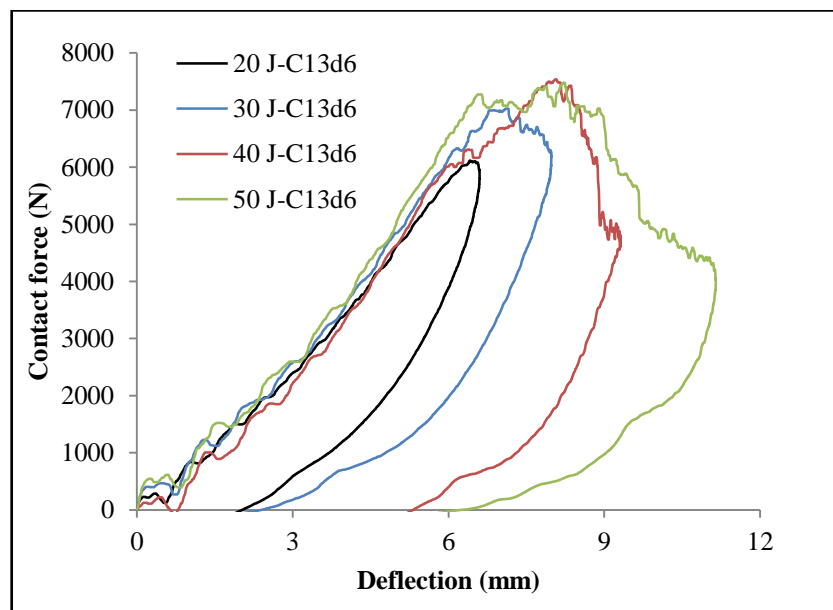
(a)
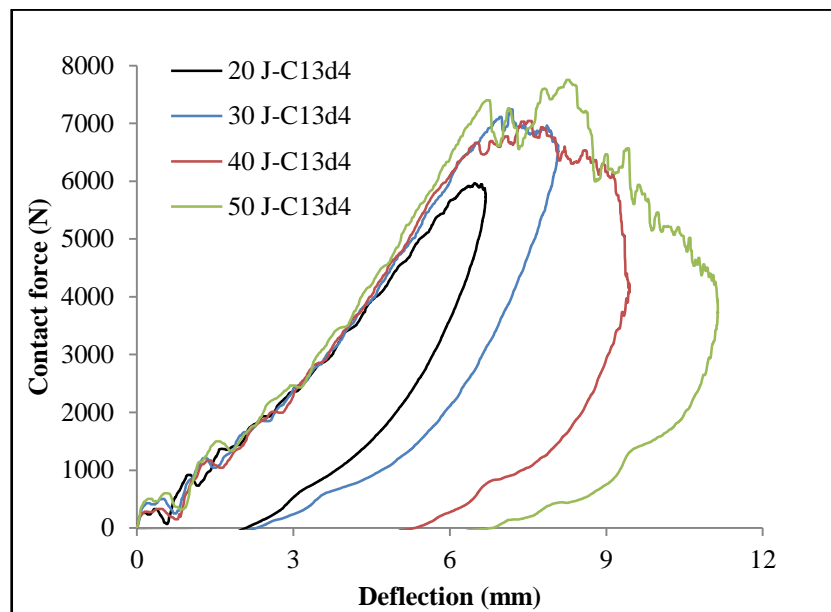
(b)

Figure 4.2 (a) The contact force-time and (b) the contact force-deflection history for specimens of C13d4 for the all energy level
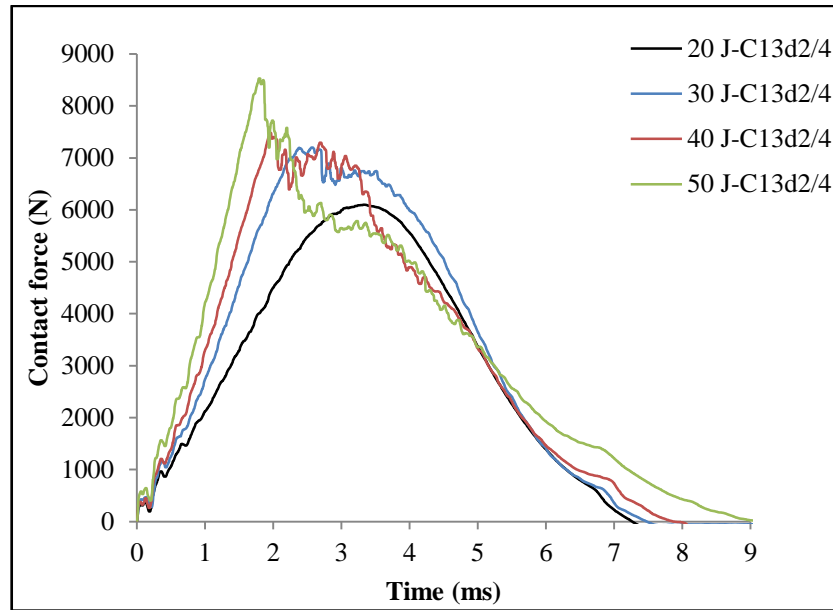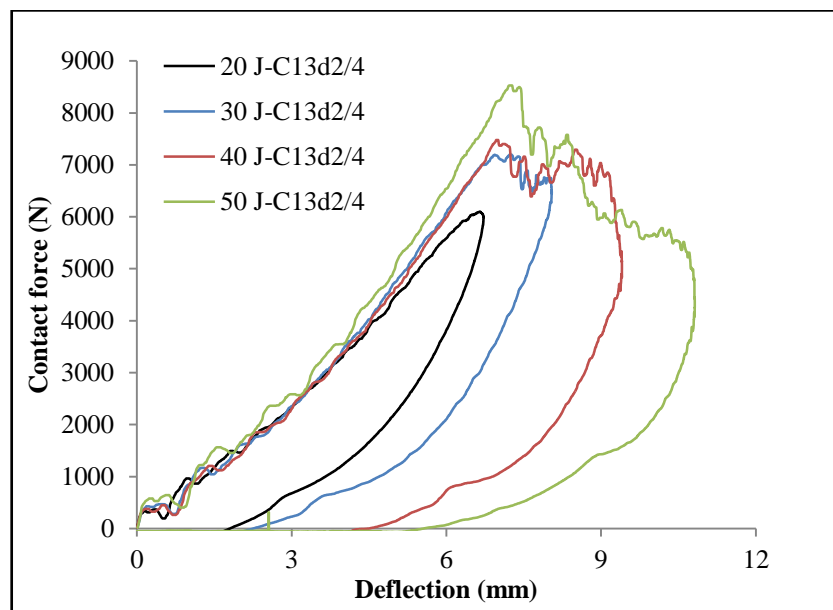
(a)

(b)

Figure 4.3 (a) The contact force-time and (b) the contact force-deflection history for specimens of C13d6 for the all energy level
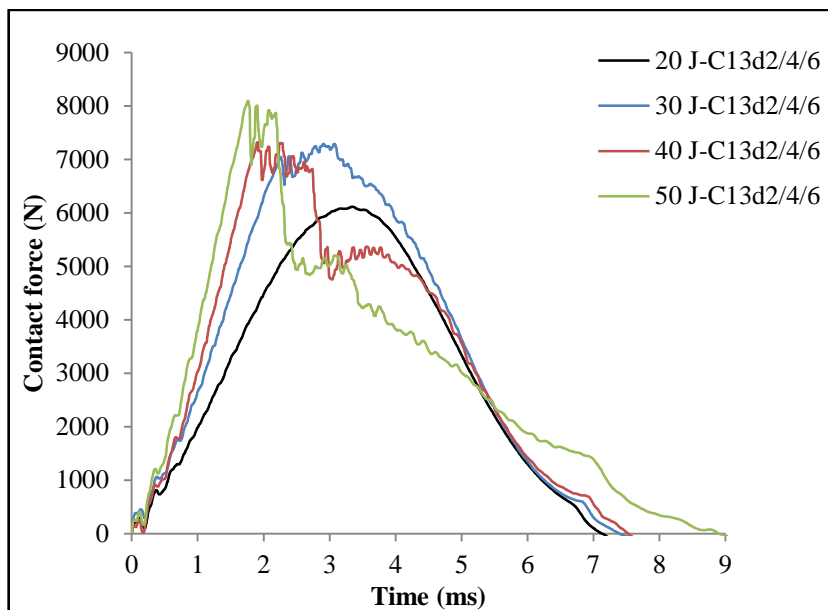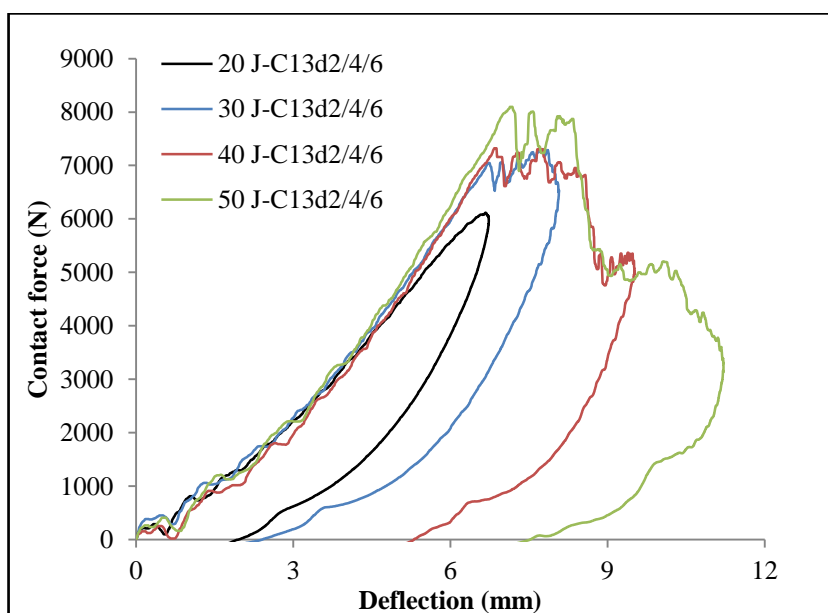
(a)

(b)

Figure 4.4 (a) The contact force-time and (b) the contact force-deflection history for specimens of C13d2/4 for the all energy level
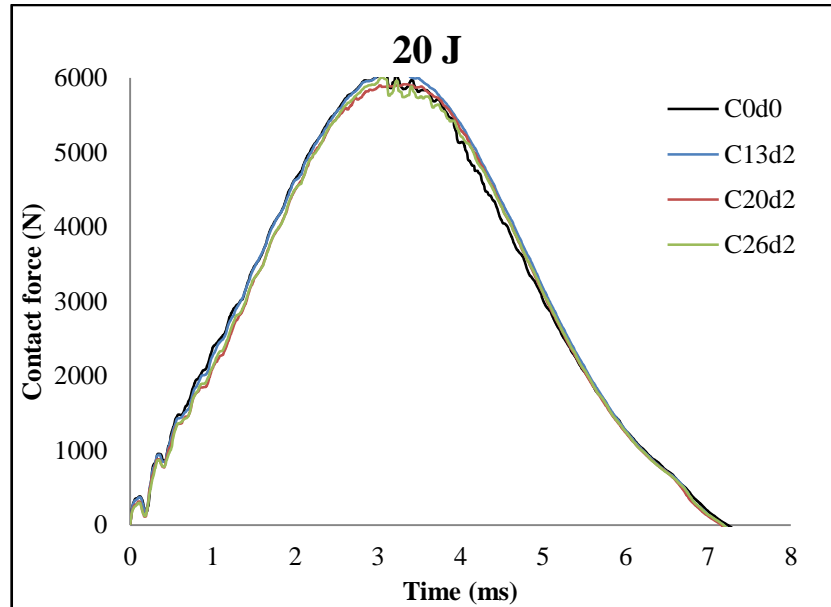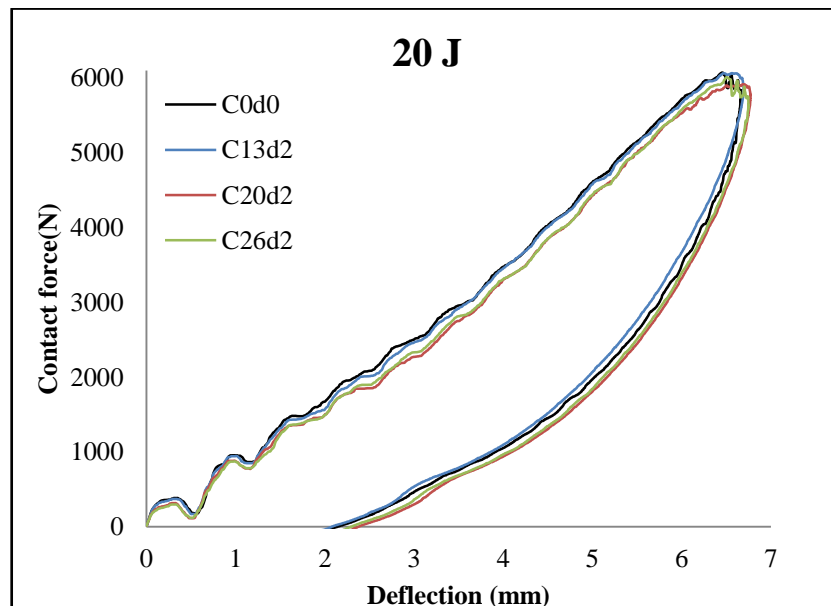
(a)

(b)

Figure 4.5 (a) The contact force-time and (b) the contact force-deflection history for specimens of C13d2/4/6 for the all energy level

4.3 Effect of Size of Delamination on Impact Behavior

Figure 4.6.a-b represents the contact force-time and contact force-deflection history depending on size of delamination at the energy level of 20 J.

(a)

(b)

Figure 4.6 (a) The contact force-time and (b) the contact force-deflection history at the energy level of 20 J for each specimen

As seen in the Figure 4.6.a, the maximum contact force is obtained as the delamination size of 13 mm. It can be said that the size of delamination has little effects on the maximum contact force value at the energy level of 20 J. And also, there is a little difference between the peak time values which is determined at the maximum contact force value. From the Figure 4.6.a-b, the curves are followed parallel to each other in both loading and unloading part of the graphics. This can be comment that the bending stiffness of specimen is the same.

From the Figure 4.6.a-b, there is no fluctuation in the both the contact force-time and the contact force-deflection curves, and they are nearly defined linear; thus, it states that only small matrix cracks and a small area of delamination are occurred into the specimen after the impact event. As shown in Figure 4.6.a-b, in loading part, the curve of the contact force-time returns parallel to the loading part. According to this, the deflection of specimen can be defined as rebounding case.

Figure 4.7.a-b is given for energy level of 30 J to show the effect of the delamination size on the impact response of each specimen. These figures represent the contact force-time and the contact force-deflection curve, respectively.

As seen in the Figure 4.7.a, the maximum contact force is detected for C13d2 at the energy level of 30 J. It can be seen that the size of delamination has an effect on the impact response of specimen. There is a little change between the maximum contact force values for each specimen. The curves of the contact force-time are nearly the same in the loading part. So, this means that bending stiffness is the same for specimen.

The maximum deflection value is observed for C20d2. In addition to this, energy level of 30 J is determined as the rebounding damage mode owing to the curves is returned parallel to the loading part compare to the unloading part.
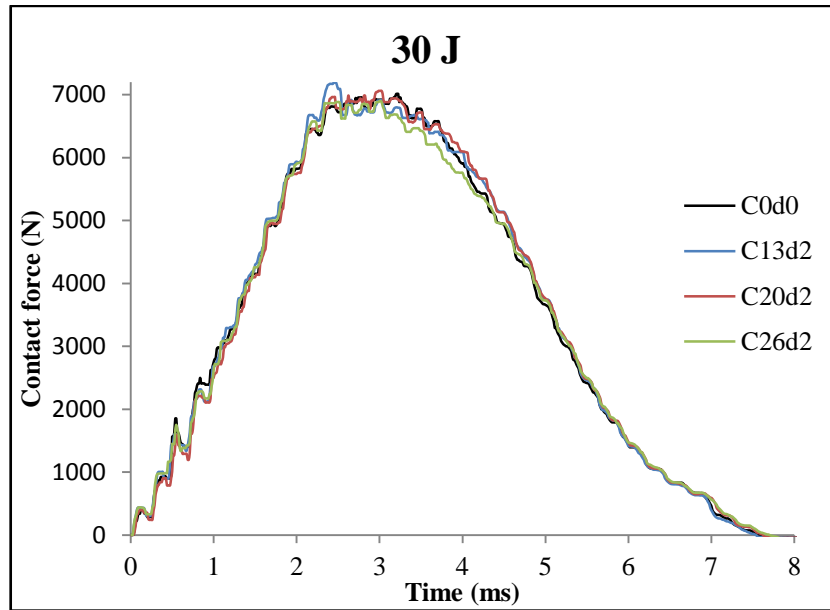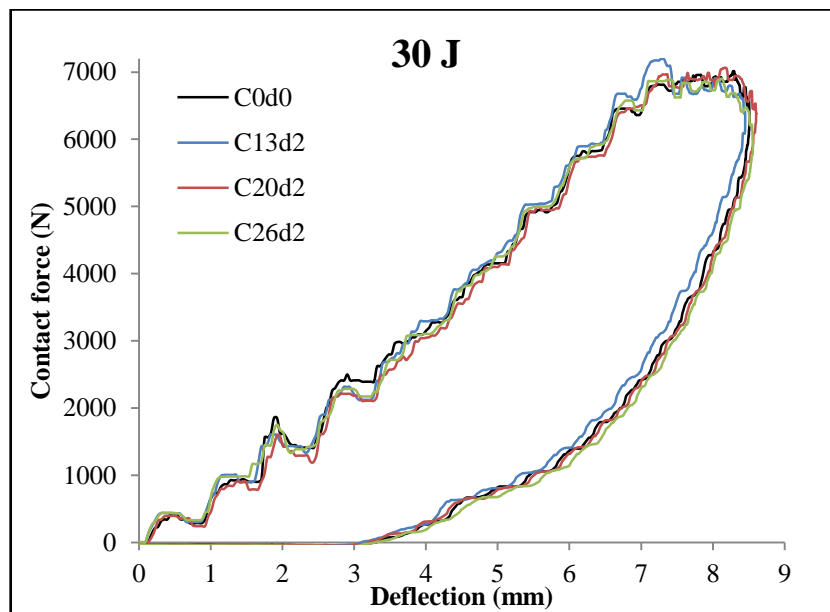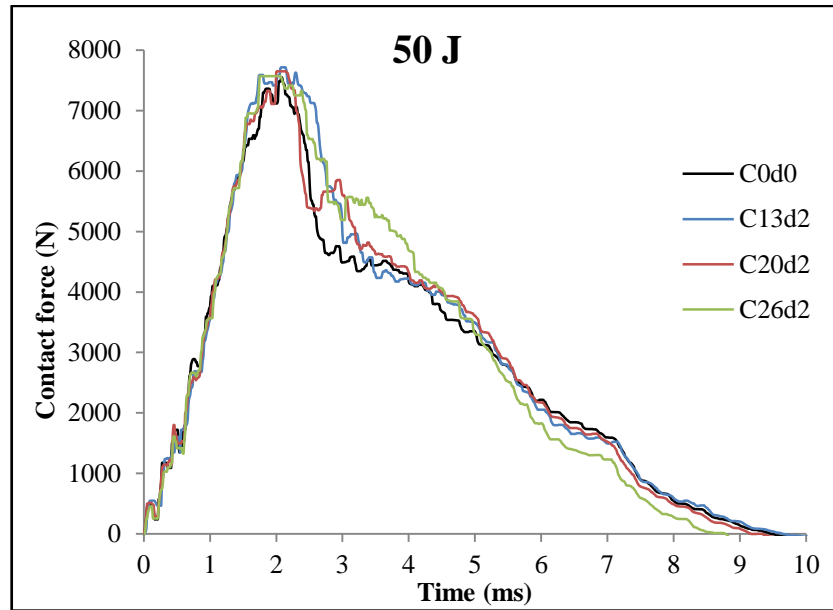
The contact force-time and the contact force-deflection curves are given in Figure 4.8.a-b for the energy level of 50 J. The maximum contact force value is occurred in case of the diameter of 20 mm between the sizes of delamination. It can be said that the size of delamination has little effect on the impact response of specimen.

From the Figure 4.8.a, among curve of all specimens, there is no significantly change between the maximum contact force values for each size of delamination at the energy level of 50 J. In loading part, the curves act together in the same way up to the maximum contact force value. So, it can be said that the specimen bending stiffness is also the same. There is a slightly difference for the bending stiffness of the specimens depending on the size of delamination.

In Figure 4.8.b, absorbed energy is increased by increasing energy level compare to the energy level of 20 J and 30 J depending on the area under the contact force-deflection curve. Also, the damage area is greater than the energy level of 20 J and 30 J because of increasing the absorbed energy. From the shape of the contact force-deflection curve, in addition to occurred matrix cracks and delamination into the specimen, it can be comment that fiber fractures are started due to fluctuation in the curve. Consequently, it can be expressed that the damage area which occurred in non-impacted surface of specimen is bigger than the impacted surface by existing the bending and delamination at the bottom surface. It is clear from the Figure 4.8.a-b that the contact time is raised by increasing the impact energy compare to the previous energy levels.

In view of the Figure 4.8.a-b, in unloading part the curves do not return the parallel to the loading part. And there is a fluctuation among the curve of the contact force-time and the contact force-deflection, but the curve is closed; thus, it can be comment that the rebounding damage mode is occurred at the energy level of 50 J. There are distinctions between the shapes of the curves arising from the existing of the difference damage mode which is occurred while the impactor is acting the reverse impact direction.
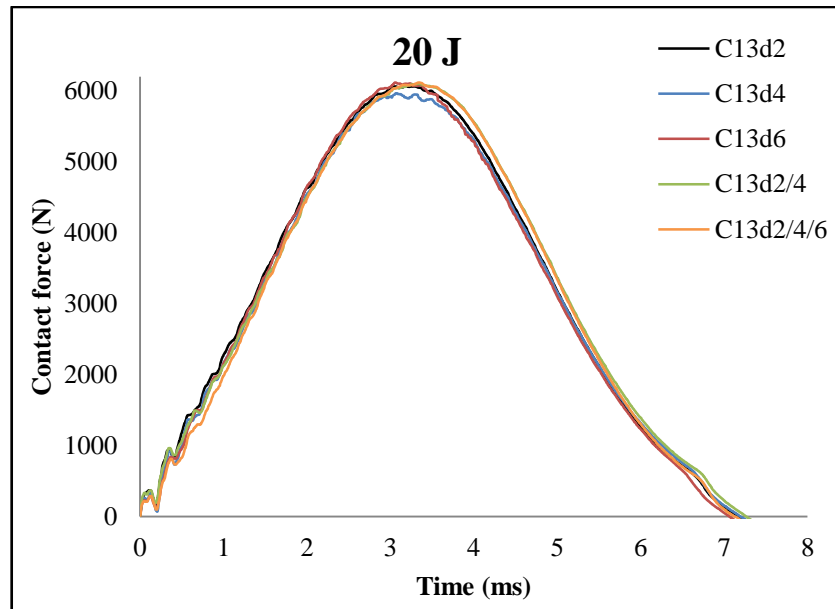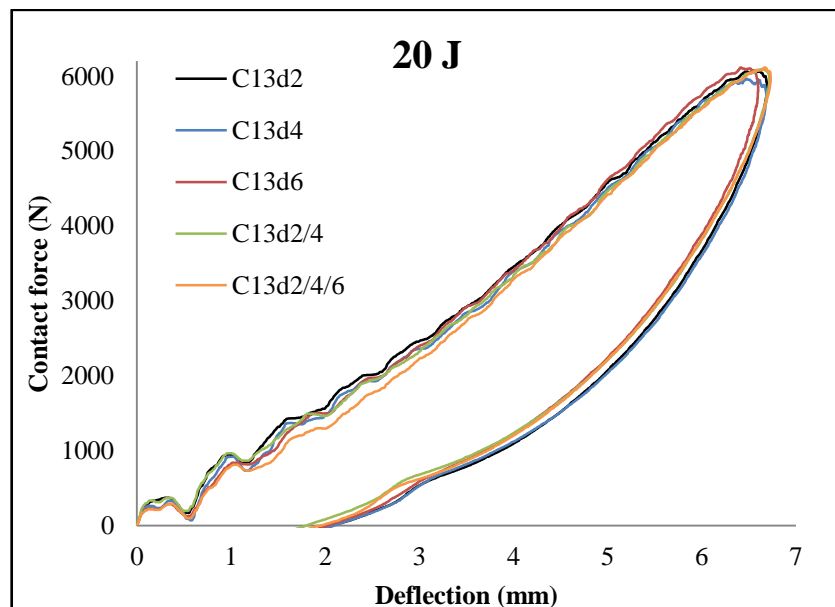
(a)
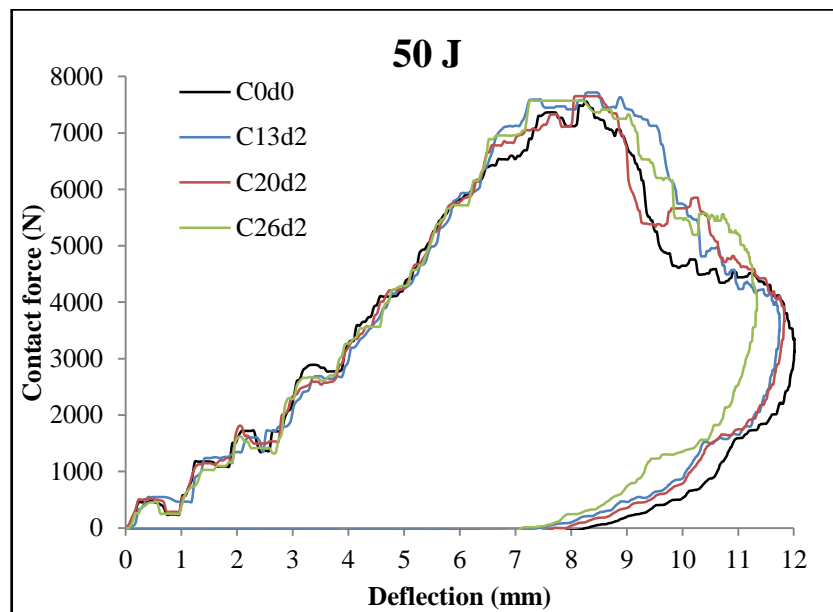
(b)

Figure 4.8 (a) The contact force-time and (b) the contact force-deflection history at the energy level of 50 J for all size of delamination

4.4 Effect of Location of Delamination on Impact Behavior

Figure 4.9.a-b shows the contact force-time and the contact force-deflection curve for location of delamination at the energy level of 20 J.

(a)

(b)

Figure 4.9 (a) The contact force-time and (b) the contact force-deflection history at the energy level of 20 J for all location of delamination

In Figure 4.9.a, the maximum contact force is observed for specimen of C13d2/4/6 at the energy level of 20 J. It can be seen that from the Figure 4.9.a, the location of delamination has little influence on the maximum contact force value at the energy level of 20 J. Besides, there is a little difference among the peak time value. From the Figure 4.9.a-b, in case of the loading and unloading time, the curves are seen to be parallel to among them; thus, it can be expressed that the bending stiffness of specimen is the same. And also, the maximum deflection is occurred for specimen of C13d2/4/6 at the energy level of 20 J.

As seen the Figure 4.9.a-b, there is no fluctuation in the curves of the contact force-time and the contact force-deflection, and they can be identified as linear. In this context, it can be said that only small matrix cracks and a small area of delamination is observed into the specimen when the impact event performed.

As shown in Figure 4.9.a-b, in loading part, the curve of the contact force-time returns parallel to one another. Consequently, it can be comment that the deflection of specimen can be defined as rebounding case.

Figure 4.10.a-b shows the contact force-time and the contact force-deflection curve for all specimens which have a delamination in the different interface from the bottom layer at the energy level of 30 J, respectively.

From the Figure 4.10.a, the maximum contact force is determined for specimen of C13d2/4/6 at the energy level of 30 J. There is a little change among the maximum contact force value for each specimen. Besides, the maximum deflection is detected for C13d2; thus, it can be said that the location of delamination has an effect on the impact response of specimen. As seen in the Figure 4.10.b, the curve is nearly the same up the maximum contact force value. So, bending stiffness is the same for specimen. In addition to this, rebounding is occurred at the energy level of 30 J.
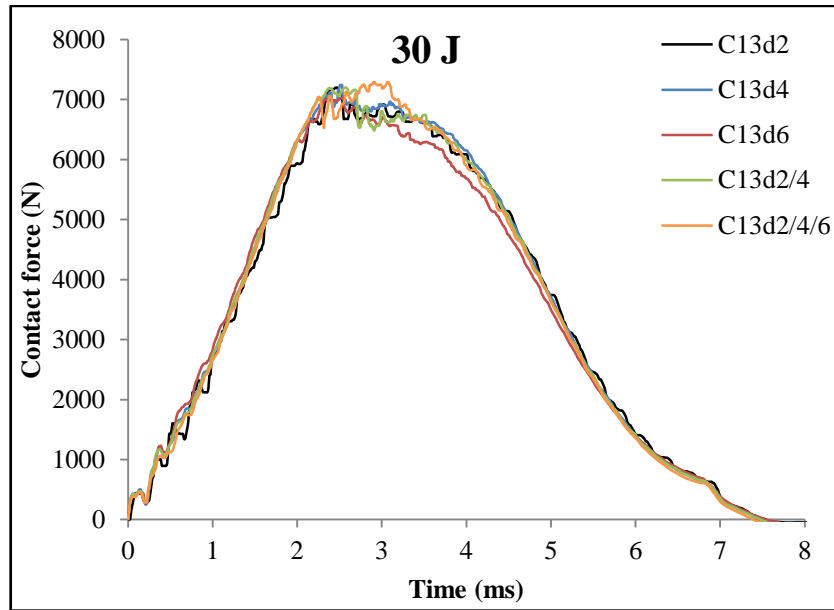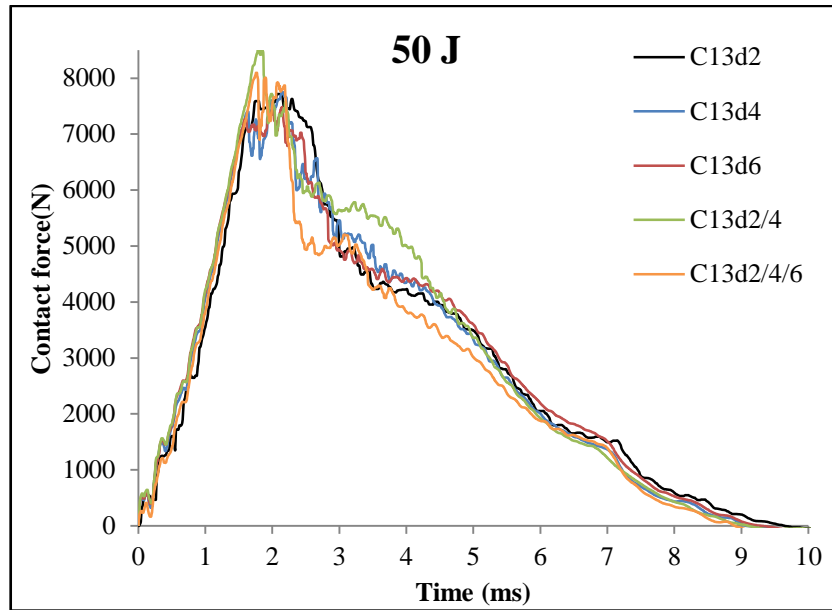
(a)
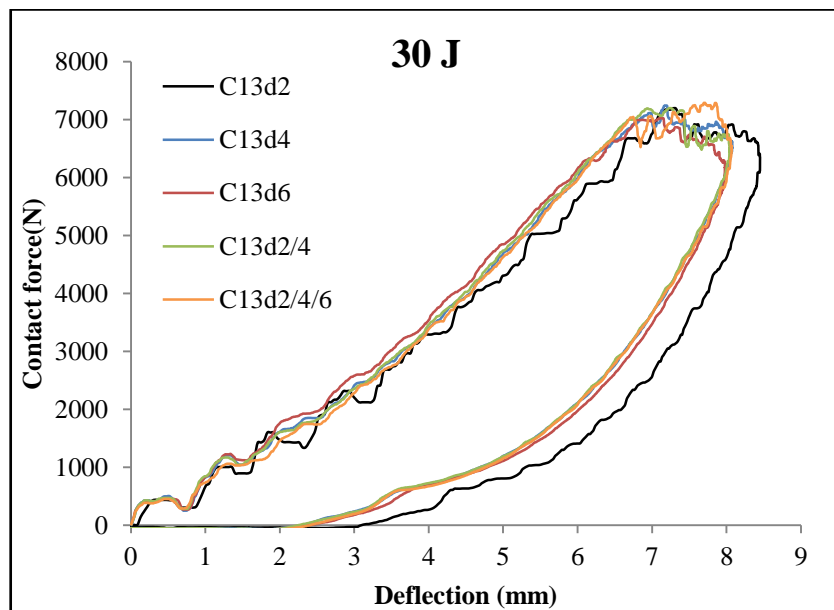
(b)

Figure 4.10 (a) The contact force-time and (b) the contact force-deflection history at the energy level of 30 J for all location of delamination
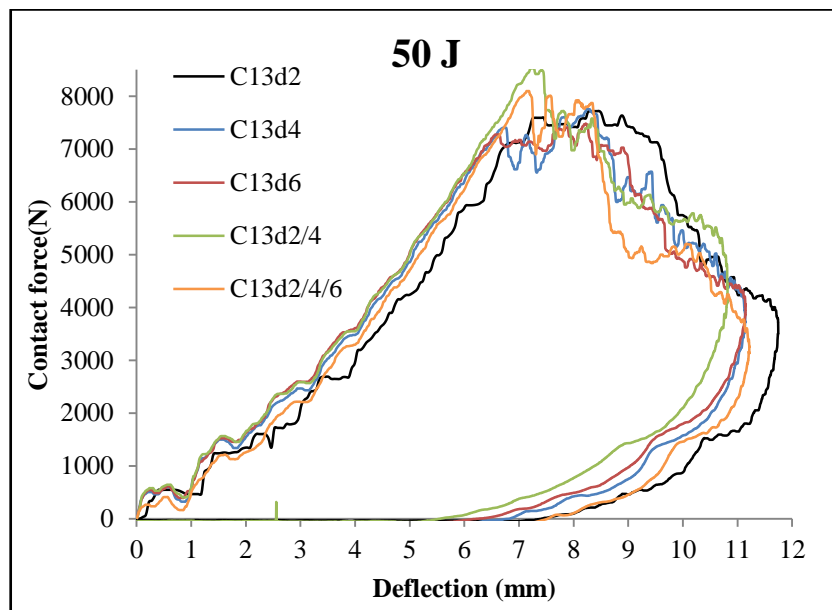
The contact force-time and the contact force-deflection curves are given in Figure 4.11.a-b for the energy level of 50 J. The maximum contact force value is occurred for specimen of C13d2/4 among the locations of delamination.

From the Figure 4.11.a, between curves of all specimens, there are differences between the maximum contact force values for each location of delamination at the energy level of 50 J. In loading part, the curves act together in the same way up to the maximum contact force value. So, it can be said that the specimen bending stiffness is also the same. There is a little distinction for the bending stiffness of the specimens due to the location of delamination. In Figure 4.11.b, absorbed energy is increased by increasing energy level compare to the energy level of 20 J and 30 J due to the area under the contact force-deflection curve. Also, the damage area is greater than the energy level of 20 J and 30 J because of increasing the absorbed energy. From the contact force-deflection curve, in addition to occurred matrix cracks and delamination into the specimen, it can be comment that fiber fractures are started due to different damage modes is occurred into the specimen after the impact event. In this context, it can be expressed that the damage area which occurred in non-impacted surface of specimen is bigger than the impacted surface by existing the bending and delamination at the bottom surface. It is clear from the Figure 4.11.a-b that the contact time is raised by increasing the impact energy compare to the previous energy levels.

As seen in Figure 4.11.a-b, in unloading part, the curves do not return the parallel to the loading part. And there is a fluctuation between the curves of the contact force-time and the contact force-deflection, but also the curve is closed; thus, it can be comment that the rebounding damage mode is occurred at the energy level of 50 J. There are differences among the shapes of the curves arising from the existing of the difference damage mode which is occurred while the impactor is moving the reverse impact direction. From the Figure 4.11.a-b, consequently, it can be said that the location of delamination has an effect on the impact behavior of composite specimen.

(a)

(b)

Figure 4.11 (a) The contact force-time and (b) the contact force-deflection history at the energy level of 50 J for all location of delamination

To make easy understanding the size and location of delamination influence on the impact behavior of laminated composite; maximum value of the contact force, contact time, and deflection are given in Figure 4.12-17 depending on the size and location of delamination at the all impact energies. Figure 4.12-13 represent the maximum contact force-impact energy diagram for the different size and location of delamination at the all impact energy level, respectively.
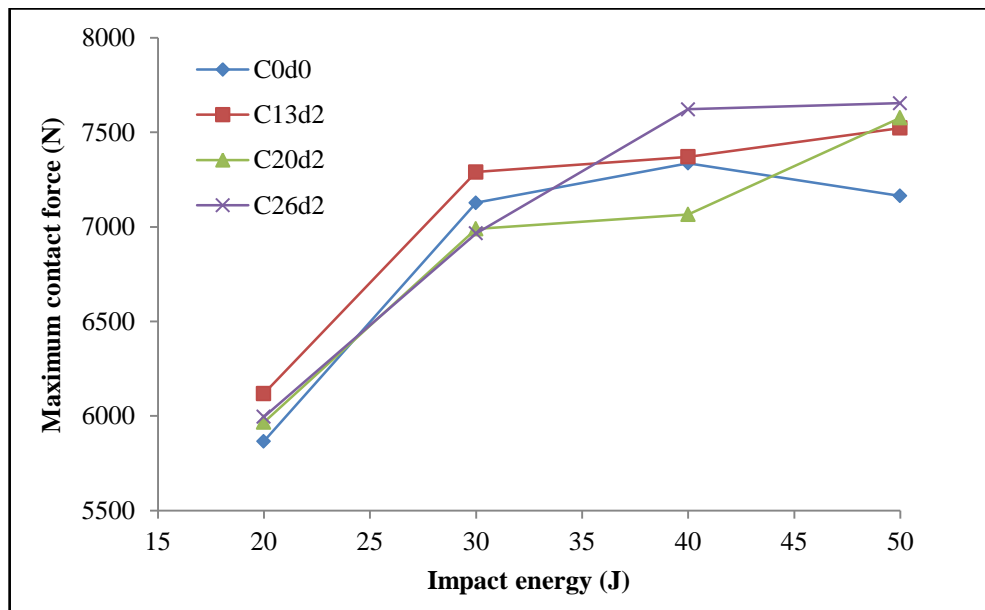

Figure 4.12 The maximum contact force-impact energy diagram depending on the size of delamination

From the Figure 4.12, the curves of the maximum contact force rises quickly until the energy level of 30 J. But, from the Figure 4.12-13, for the greater energy level than the 30 J, the maximum contact force increases with less slopping depending on the size and location of delamination. It can be expressed that fiber breakage occurs addition to matrix cracks and delamination after the impact energy level of 30 J up to the 50 J; thus, there is a fluctuation in the curves of the maximum contact force. As seen in the Figure 4.12-13, the lowest value of the maximum contact force is occurred for specimen of C0d0 and C13d4, respectively. In Figure 4.12, the maximum value of the maximum contact force is observed for specimen of C26d2 compare to the other size of delamination.

It can be comment that C26d2 is more rigid than others. In the same way, in Figure 4.13, specimen of the C13d2/4 is seen to be more rigid than the others.
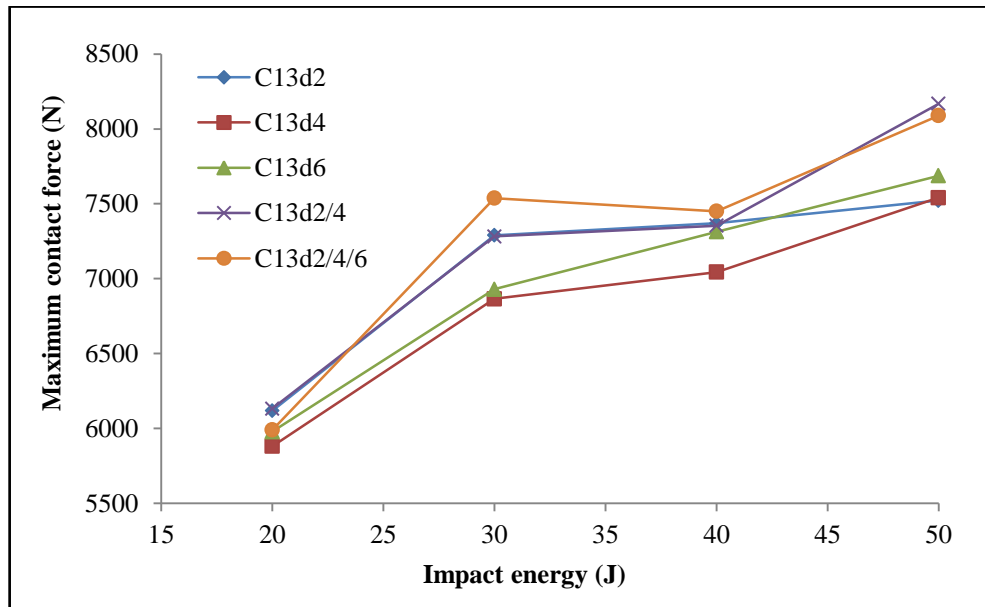

Figure 4.13 The maximum contact force-impact energy diagram depending on the location of delamination

Figure 4.14-15 illustrate the contact time-impact energy diagram depending on the size and location of delamination at the different energy level, respectively. From Figure 4.14, there is a little change between the curves of the contact time-impact energy up to the energy level of 30 J. This result can be comment that the energy range is called rebounding energy level. The prevalent damage mode can be defined as delamination. Besides, it can be comment that delamination is decreased by increasing the contact time. And also, the contact time is progressively raised range from 30 J to 50 J. In this range of energy level, rebounding is prevalent damage mode. The maximum value of the contact time is observed for C0d0 depending on the size of delamination and is determined for C13d4 depending on the location of delamination at the energy level of 50 J.
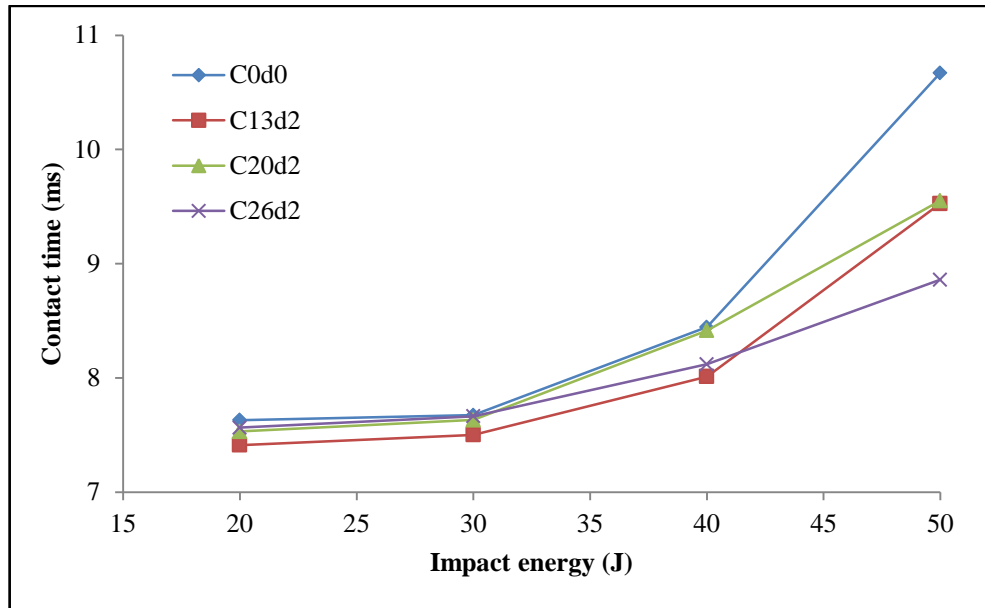
Figure 4.14 The contact time-impact energy diagram depending on the size of delamination
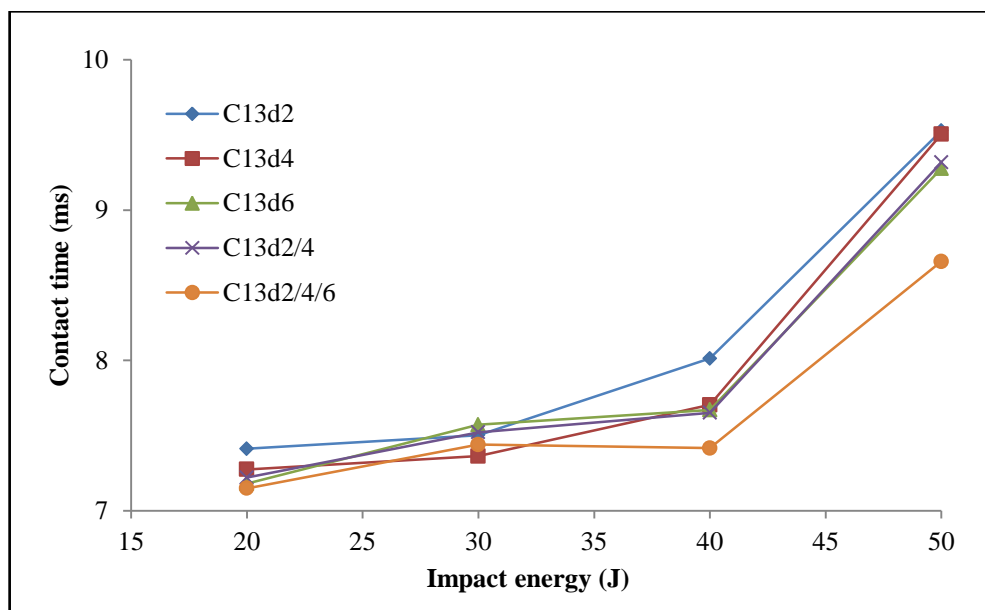

Figure 4.15 The contact time-impact energy diagram depending on the location of delamination

Figure 4.16-17 show the maximum deflection-impact energy diagram depending on the size and location of delamination at the different impact energy level. In Figure 4.16-17, the curve of the maximum deflection-impact energy can be defined as nearly linear except for among of 40 J and 50 J depending on both size and location of embedded delamination. So, it can be said that there is no substantially

different between the curves of the maximum deflection-impact energy depending on the size and location of delamination. It can be expressed that the value of maximum deflection is defined as nearly the same depending on size and location of delamination.
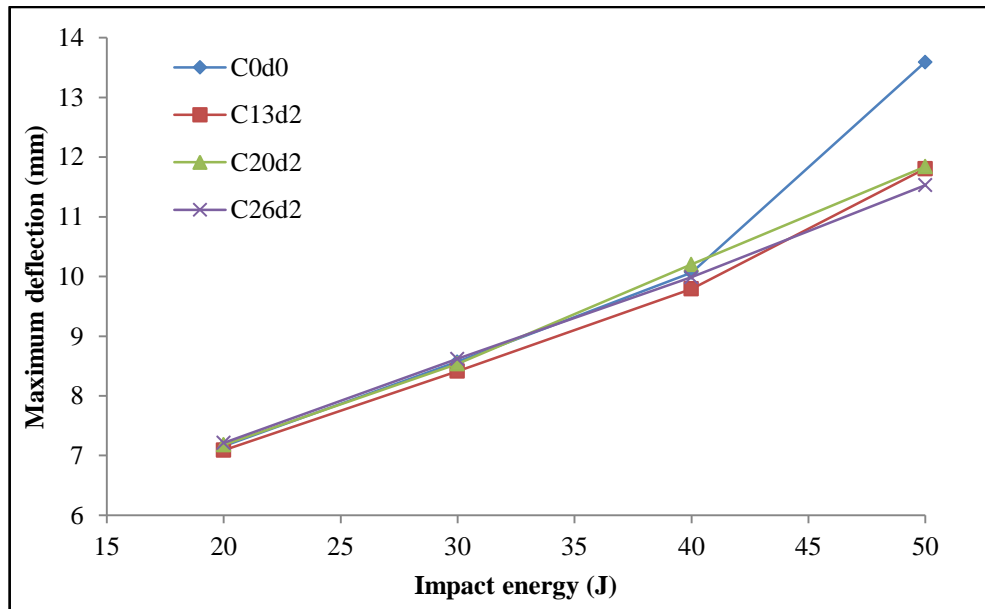

Figure 4.16 The maximum deflection-impact energy diagram depending on the size of delamination
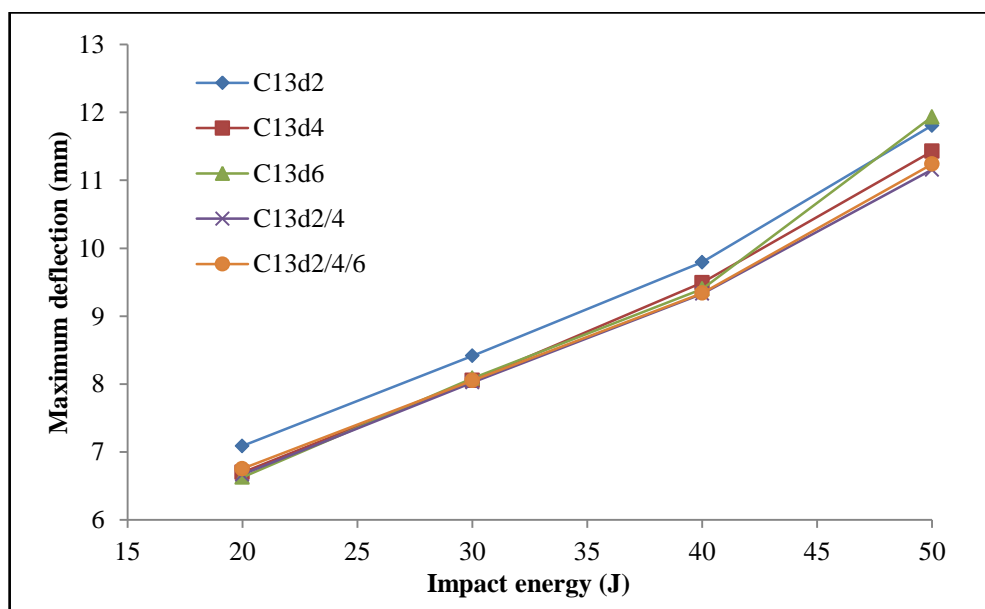

Figure 4.17 The maximum deflection-impact energy diagram depending on the location of delamination

Figure 4.18-19 show the absorbed energy-impact energy diagram depending on the size and location of delamination for all energy level, respectively. Both impact energy (E_i) and absorbed energy (E_a) are two mainly factor to evaluate the impact behavior of laminated composite. The impact energy is defined as the amount of total energy initially applied to specimen. The impact energy which is absorbed by specimen is called the absorbed energy. Energy profile diagram is showed that relationship between the impact energy and the absorbed energy is given in Figure 4.18-19. The relationship between the absorbed energy-impact energy is shown in a diagram which is called energy profile diagram. From the Figure 4.18-19, it is seen that the absorbed energy is raised by the increasing the impact energy level. In Figure 4.18, the maximum value of the absorbed energy is observed for specimen of C0d0, which has no embedded delamination, depending on the size of delamination at the energy level of 50 J. From the Figure 4.19, the maximum value of the absorbed energy is determined for C13d2 due to location of delamination at the energy level of 50 J. And also, it can be defined that the rebounding is occurred at the all energy level.
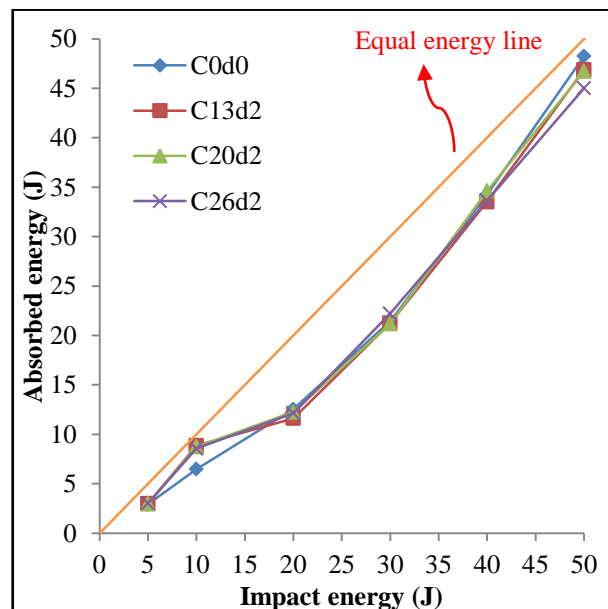

Figure 4.18 The absorbed energy-impact energy diagram depending on the size of delamination for all energy level
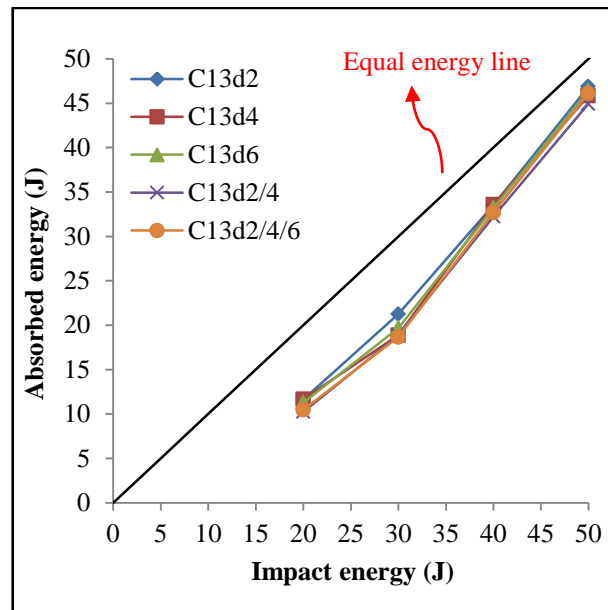
Figure 4.19 The absorbed energy-impact energy diagram depending on the location of delamination for all energy level

Figure 4.20-21 show that the changing of the absorbed energy depending on the size and location of delamination for all energy level, respectively. As seen in the Figure 4.20, the absorbed energy is nearly constant for each specimen at the energy level of 5 J. But, the maximum value of the absorbed energy occurs for specimen manufactured without delamination at the energy level of 50 J; thus, this result can be comment that the damage area is greater than the other specimen due to the size of delamination at the energy level of 50 J. In Figure 4.20, it can be seen that there is little difference between the maximum values of the absorbed energy depending on the size of delamination for the same energy level.

From the Figure 4.21, the maximum value of the absorbed energy is seen to be determining for specimen of C13d2 at the energy level of 50 J. This is an expected result owing to the increasing energy level. As seen in the Figure 4.21, it can be said that the specimen of C13d2 has greatest damage area than the other specimen depending on the location of delamination at the energy level of 50 J.
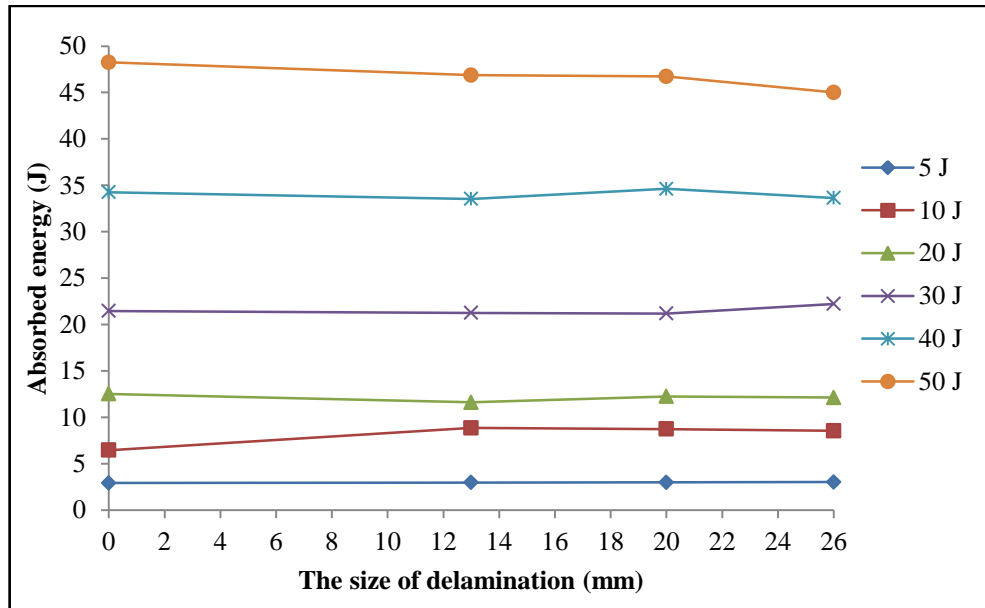
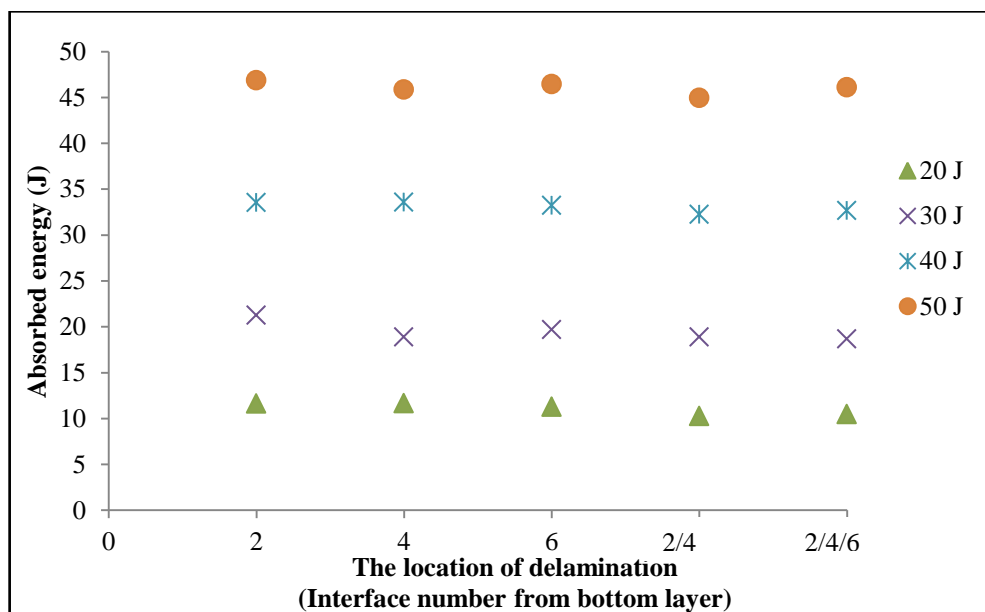Figure 4.20 The absorbed energy-size of delamination diagram for all energy level

Figure 4.21 The absorbed energy-location of delamination diagram for all energy level

4.5 Damage Photos of the Test Specimens

In this subsection, damage photos are given to show the damage area and determine the damage mode with the aid of high intensity backlighting after the impact test for specimen at the energy level of 20 J, 30 J and 50 J.

Figure 4.22-23 are given to show the photo of damaged specimen depending on the size and location of delamination at the energy level of 20 J, respectively. In these figures, it can be said that small matrix crack and delamination is observed for each specimen. The damage area is nearly the same the embedded delamination which size is 13 mm. And also, the damage area is smaller than the other embedded delamination size of 20 mm and 26 mm.
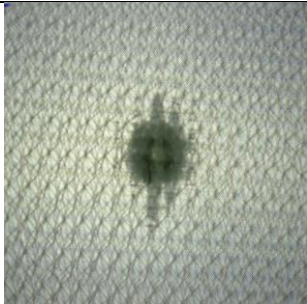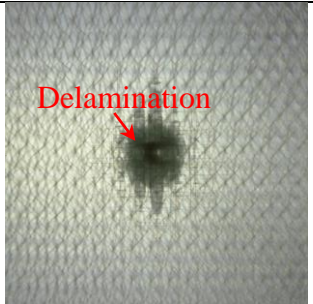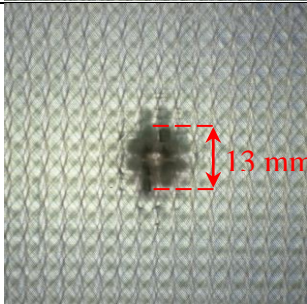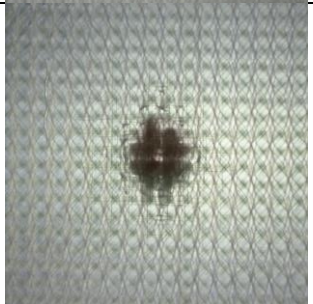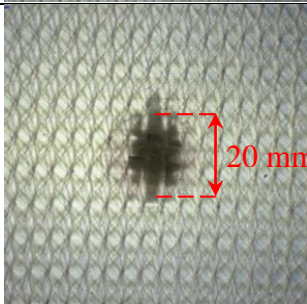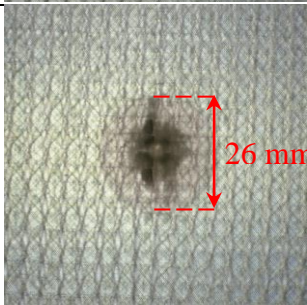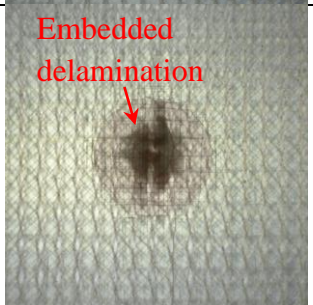
Figure 4.22 Damage photos of specimen due to the size of delamination at the energy level of 20 J
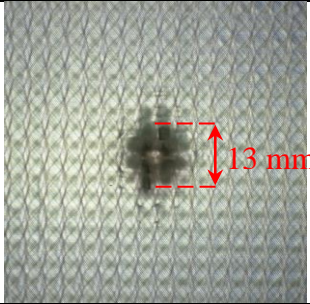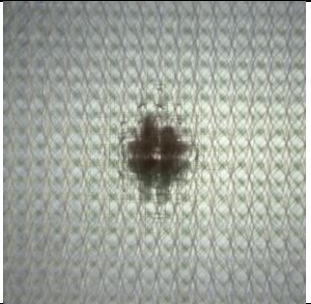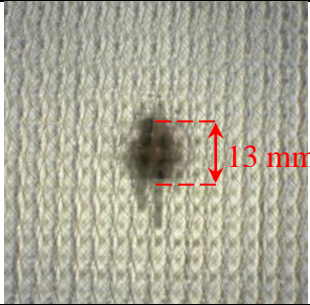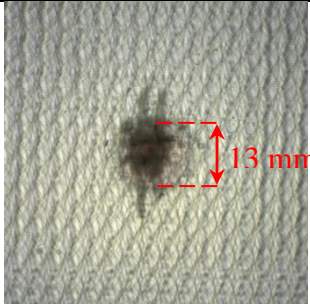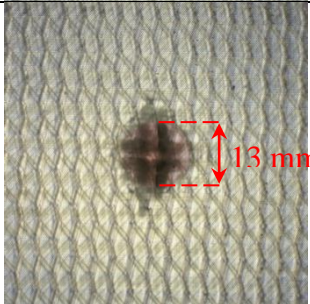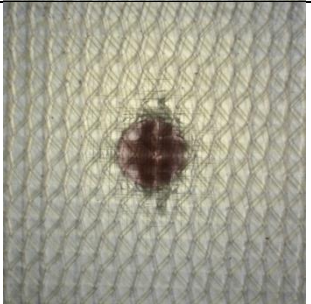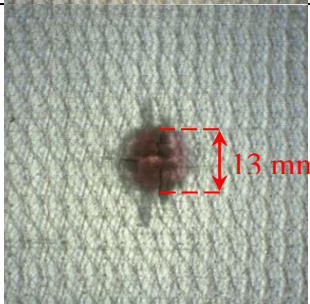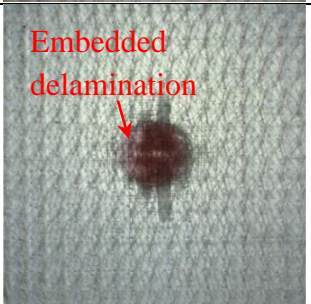
	Material Properties	Top	Bottom
20J	C13d2	13 mm	
	C13d4	13 mm	
	C13d6	13 mm	Delamination
	C13d2/4	13 mm	
	C13d2/4/6	13 mm	Embedded delamination

Figure 4.23 Damage photos of specimen due to the location of delamination at the energy level of 20 J

Figure 4.24-25 show the photos of damaged specimen due to the size of delamination at the energy level of 30 J. From these figures, small matrix cracks and delamination is detected for each specimen. Delamination area is nearly the same the size of delamination which is 13 mm. Besides, it can be comment that the damage area at the 30 J may be greater than at the 20 J. The main damage mode is observed as delamination and matrix cracks.
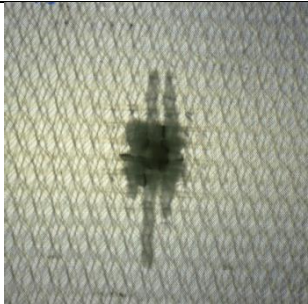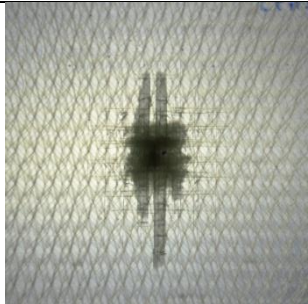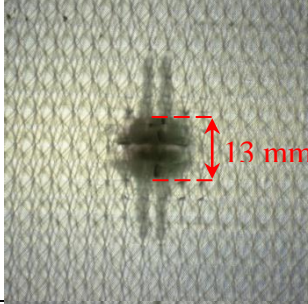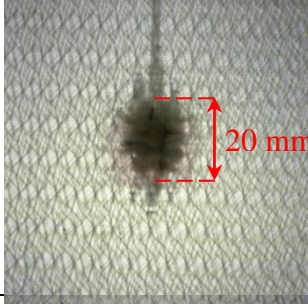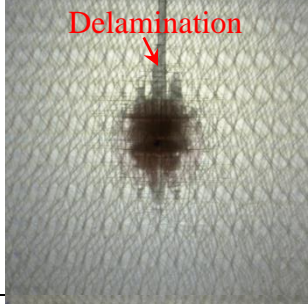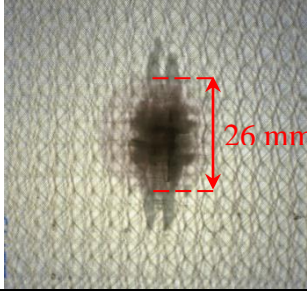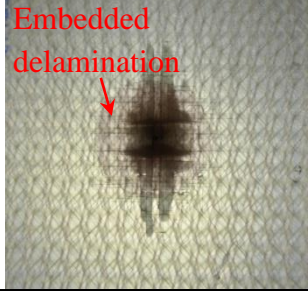
Figure 4.24 Damage photos of specimen due to the size of delamination at the energy level of 30 J

Material Properties	Top	Bottom
C13d2	13 mm	
C13d4	13 mm	
C13d6	13 mm	
C13d2/4	13 mm	
C13d2/4/6	13 mm	

30J
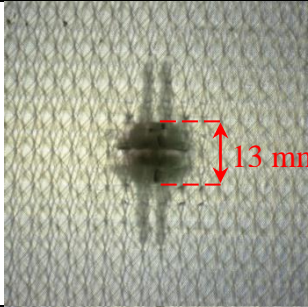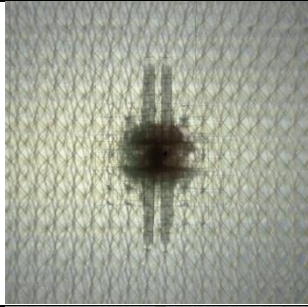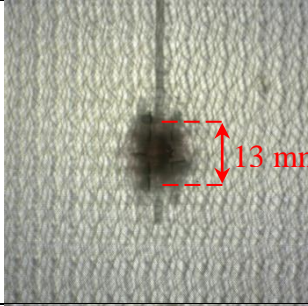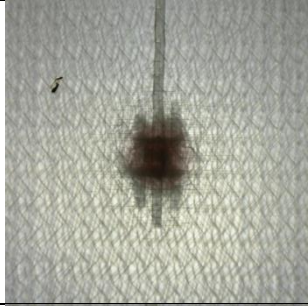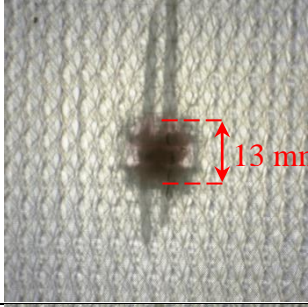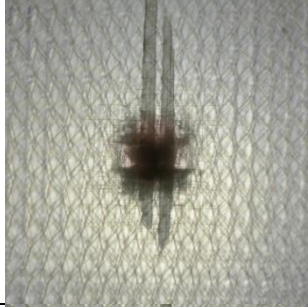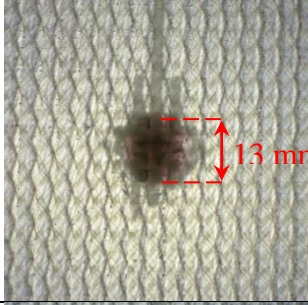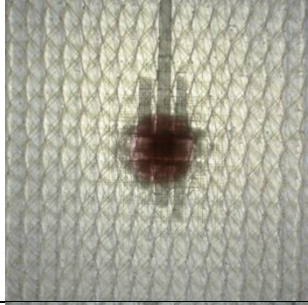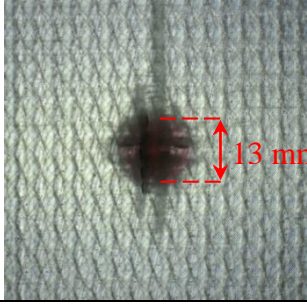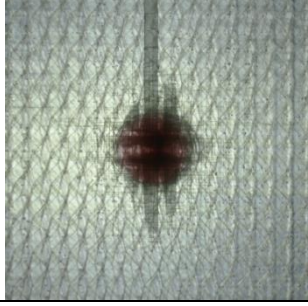
Figure 4.25 Damage photos of specimen due to the location of delamination at the energy level of 30 J

Figure 4.26-27 represent the photos of the damaged specimen due to the size and location of delamination at the energy level of 50 J, respectively. In these figures, damage area is greater than the energy level of 20 J and 30 J because of the increasing the absorbed energy. Damage area is seen to be same the size of delamination of 20 mm. It can be said that fiber breakage is observed allied with delamination and matrix cracks.
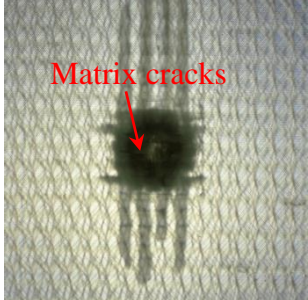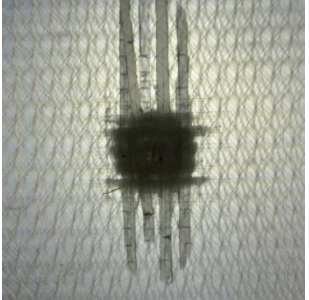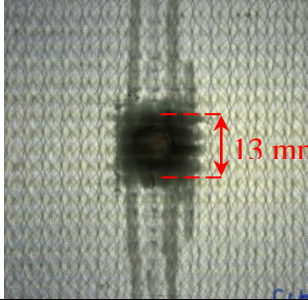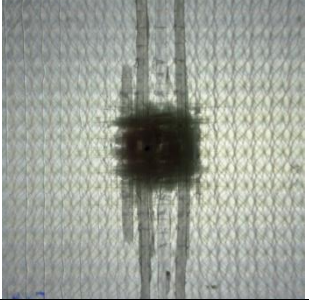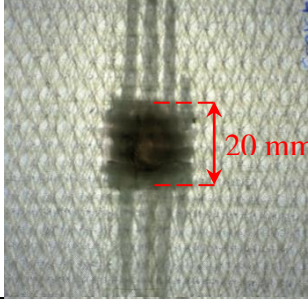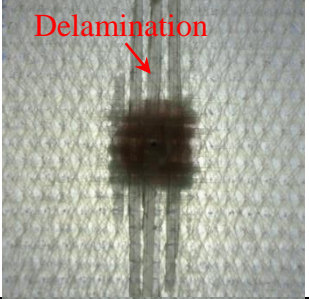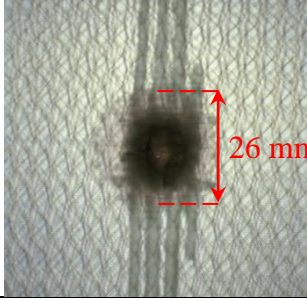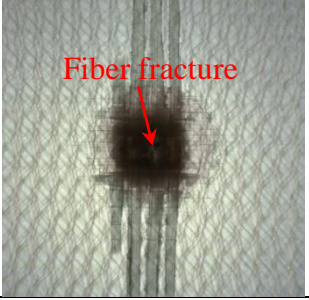
Figure 4.26 Damage photos of specimen due to the size of delamination at the energy level of 50 J
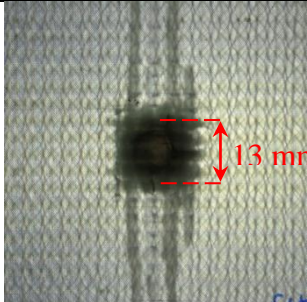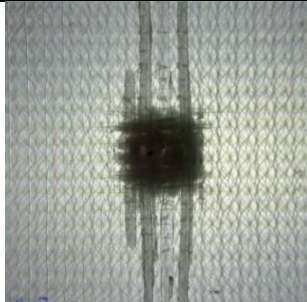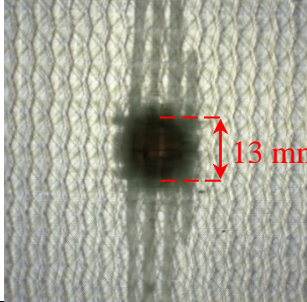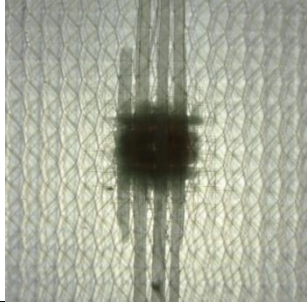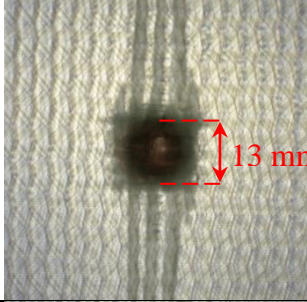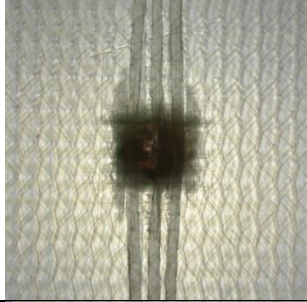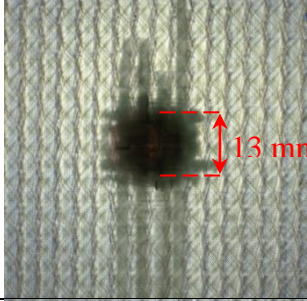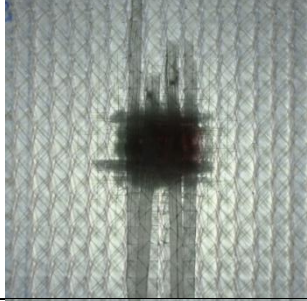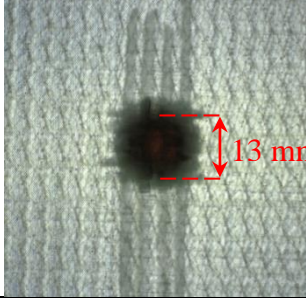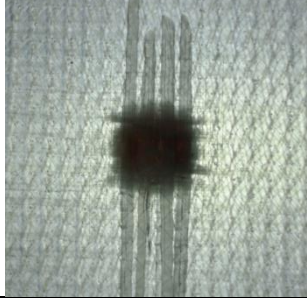
Material Properties		Top	Bottom
50J	C13d2	13 mm	
	C13d4	13 mm	
	C13d6	13 mm	
	C13d2/4	13 mm	
	C13d2/4/6	13 mm	

Figure 4.27 Damage photos of specimen due to the location of delamination at the energy level of 50 J

CHAPTER FIVE
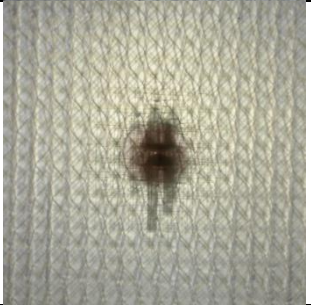## CONCLUSIONS AND RECOMMENDATIONS

In this study, the influence of size and location of embedded delamination on impact behavior of laminated composite was investigated, experimentally. From this study, the concluding remarks drawn from this study can be summarized as below:

- The contact force and impact time rise by the increasing impact energy level except for 5 J and 10 J.

- The maximum value of deflection is increased by increasing impact energy level.

- There is no significantly a difference between the values of maximum contact force and maximum deflection depending on the size of delamination.

- The location of delamination has little effect on the values of maximum contact force and maximum deflection depending on the placed interface from the bottom layer.

- The location of delamination on the impact behavior is seen to be more effective than the size of delamination.

- The common damage is observed as delamination and matrix cracks but rather fiber fractures less than roughly impact energy of 30 J. Also, there is some fiber fractures accompanied by delamination and matrix cracks for higher than approximately 40 J.

- Rebounding damage mode is observed at the all energy level.

- For lower impact energy level, the damaged area has nearly the same area due to the area of embedded delamination which size is 13 mm. However, for higher impact energy level, the damaged area is the same the area of embedded delamination which size is 20 mm.

- The maximum value of the absorbed energy is observed in experiments which performed by using the specimen of C0d0 owing to the elastic behavior of specimen depending on the size of delamination at the energy level of 50 J. Thus, it can be comment that the maximum damaged area is occurred into the specimen of C0d0.

- The maximum value of the absorbed energy is determined in experiments which performed by using the specimen C13d2 because of the elastic behavior of specimen at the energy of 50 J.

- The absorbed energy is also increased by the increasing energy level. Besides, the damaged area is increased by increasing impact energy level.

- The damaged area of impacted surface is greater than the non-impacted surface depending on the tensile crack owing to bending and delamination of bottom surface of specimen.

- Effect of embedded delamination which is placed out-of-impact point in composite may be investigated in the next.
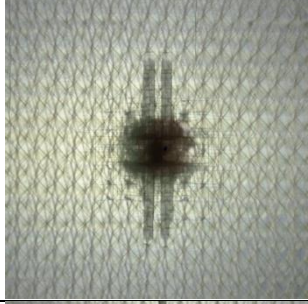
- Effect of embedded delamination which has an elliptical shape in composite may be performed in the next.

- Effect of delamination which embedded the entire interface in composite may be studied at the high impact energy level in the next.

REFERENCES

Abrate, S. (1998). *Impact on composite structures* (1st ed.). Cambridge: Cambridge University Press.

Abrate, S. (2011). *Impact engineering of composite structures* (1st ed.). USA: SpringerWienNewyork.

Akın C., & Senel M. (2010). An experimental study of low velocity impact response for composite laminated plates. *Journal of the Institute of Science and Technology of Dumlupınar University, 21*, 77-90.

Aktas, M., Atas C., Icten, B. M., & Karakuzu R. (2009). An experimental investigation of the impact response of composite laminates. *Composite Structures, 87*, 307–313.

Aslan, Z., Karakuzu, R., & Okutan, B. (2003). The response of laminated composite plates under low velocity impact loading. *Composite Structures, 59*, 119–127.

Aslan, Z., Karakuzu, R., & Sayman, O. (2002). Dynamic characteristics of laminated woven E-glass–epoxy composite plates subjected to low velocity heavy mass impact. *Journal of Composite Materials, 36* (21), 2421–2442.

Atas, C., & Liu, D. (2008) Impact response of woven composites with small weaving angles. *International Journal of Impact Engineering, 35*, 80–97.

Baucom, J. N., & Zikry, M. A. (2005). Low-velocity impact damage progression in woven E-glass composite systems. *Composites: Part A, 36,* 658–664.

Belingardi, G., & Vadori, R. (2002). Low velocity impact tests of laminate glass-fiber–epoxy matrix composite material plates. *International Journal of Impact Engineering, 27*, 213–229.

Caprino, G., Lopresto, V., Scarponi, C., & Briotti, G. (1999). Influence of material thickness on the response of carbon-fabric/epoxy panels to low velocity impact. *Composites Science and Technology, 59*, 2279-2286.

Cho, C., & Zhao, G. (2002). Effects of geometric and material factors on mechanical response of laminated composites due to low velocity impact. *Journal of Composite Materials, 36*, 1403–1428.

Chakraborty D. (2007). Delamination of laminated fiber reinforced plastic composites under multiple cylindrical impact. *Materials and Design, 28*, 1142–1153

Composite materials. (2012). General composites. Retrieved May 26, 2012 from http://www.efunda.com

Datta, S., Krishna, A. V., & Rao, R. M. V. G. K. (2004). Low velocity impact damage tolerance studies on glass/epoxy laminates − effects of material, process and test parameters. *Journal of Reinforced Plastics and Composites, 23* (3), 327–345.

Daniel, I. M., & Ishai, O. (1994). *Engineering mechanics of composite materials* (1st ed.). Newyork: Oxford University Press

Evci, C., & Gülgeç M. (2012). An experimental investigation on the impact response of composite materials. *International Journal of Impact Engineering, 43*, 40–51.

Freitas, M., Silva, A., & Reis, L. (2000). Numerical evaluation of failure mechanisms on composite specimens subjected to impact loading. *Composite Part B, 31* (3), 199–207.

Fuossa E., Straznickya P. V., & Peon, C. (1998). Effects of stacking sequence on the impact resistance laminates - Part 1: parametric study. *Composite Structures, 41*, 67-77.

Fuossa E., Straznickya P. V., & Peon, C. (1998). Effects of stacking sequence on the impact resistance laminates. Part 2: prediction method. *Composite Structures, 41*, 177-186.

Goren A., & Atas, C. (2008). Manufacturing of polymer matrix composites using vacuum assisted resin infusion molding. *Archives of Materials Science and Engineering, 34* (2), 117–120

Hosur, M. V., Abdullah, M., & Jeelani, S. (2005). Studies on the low-velocity impact response of woven hybrid composites. *Composite Structures, 67* (3), 253–262.

Icten, B. M., Atas C., Aktas, M., & Karakuzu R. (2009). Low temperature effect on impact response of quasi-isotropic glass/epoxy laminated plates. *Composite Structures, 91*, 318–323.

Jones, R. M. (1999). *Mechanics of composite materials* (2nd ed.). UK: Taylor & Francis Inc.

Karakuzu, R., Erbil, E., & Aktas M. (2010). Impact characterization of glass/epoxy composite plates: An experimental and numerical study. *Composites: Part B, 41*, 388–395.

Kompozit malzemeler. (2008). Akıllı malzemeler. Retrieved May 26, 2012 from http://www.populerbilgi.com/genel/akilli_malzemeler.php

Li, C. F., Hu, N., Cheng, J. G., Fukunaga, H., & Sekine, H. (2002). Low-velocity impact-induced damage of continuous fiber-reinforced composite laminates. Part II. Verification and numerical investigation. *Composites Part A, 33* (8), 1063–1072.

Liu D. (2004). Characterization of impact properties and damage process of glass/epoxy composite laminates. *Journal of Composite Materials, 38*, 1425–1442.

Mazumdar, S. K., (2002) *Composites manufacturing: materials, product, and process Engineering*, USA: CRC Press LLC.

Mili, F., & Necib, B. (2001). Impact behavior of cross-ply laminated composite plates under low velocities. *Composite Structures, 51* (3), 237–244.

Mitrevski, T., Marshall, I. H., & Thomson, R. (2006). The influence of impactor shape on the damage to composite laminates. *Composite Structures, 76,* 116–122.

Mitrevski T., Marshall I. H., Thomson R., Jones, R., & Whittingham, B. (2005). The effect of impactor shape on the impact response of composite laminates. *Composite Structures, 67*, 139–148.

Naik, N. K., Ramasimha, R., Arya, H., Prabhu, S. V., & Shamarao N. (2001). Impact response and damage tolerance characteristics of glass-carbon/epoxy hybrid composite plates. *Composite Part B, 32*, 565-74.

Olsson, R., Donadon, M. V., & Falzon, B. G. (2006). Delamination threshold load for dynamic impact on plates. *International Journal of Solids and Structures, 43* (10), 3124–3141.

Rydin, R. W., Bushman, M. B., & Karbhari, V. M. (1995). The influence of velocity in low velocity impact testing of composites using the drop weight impact tower. *Journal of Reinforced Plastics and Composites, 14*, 113–27.

Sadasivam, B., & Mallick, P. K. (2002). Impact damage resistance of random fiber reinforced automotive composites. *Journal of Thermoplastic Composite Materials, 15*, 181–191.

Symons, D. D. (2000). Characterisation of indentation damage in 0/90 lay-up T300/914 CFRP. *Composites Science and Technology, 60*, 391-401.

Tiberkak, R., Bachene, M., Rechak, S., & Necib, B. (2008). Damage prediction in composite plates subjected to low velocity impact. *Composite Structures, 83* (1), 73–82.

Tita, V., Carvalho, J., & Vandepitte D. (2008). Failure analysis of low velocity impact on thin composite laminates: experimental and numerical approaches. *Composite Structures, 83* (4), 413–428.

Uyaner, M., & Kara, M. (2007). Dynamic response of laminated composites subjected to low-velocity impact. *Journal of Composite Materials, 41*, 2877-2895.

Whittingham, B., Marshall, I. H., Mitrevski, T., & Jones R. (2004). The response of composite structures with pre-stress subject to low velocity impact damage. *Composite Structures, 66,* 685–98.

Wu, H. Y. T., & Chang, F. K. (1989). Transient dynamic analysis of laminated composite plate subjected to transverse impact. *Composite Structures, 31*, 453–466.

Ye, J. (2003). *Laminated composite plates and shalls: 3D modelling.* UK: Springer & Verlag.

Zhang, Y., Zhu, P., & Lai, X. (2006). Finite element analysis of low-velocity impact damage in composite laminated plates. *Materials and Design, 27*, 513–519.

Zheng, D., & Binienda, W. K. (2007). Effect of permanent indentation on the delamination threshold for small mass impact on plates. *International Journal of Solids and Structures, 44*, 8143–8158.

APPENDIX

The characteristic curves of each expression of test results measured from the impact test are given in chapter of experimental results. Although the each experiment is performed five times, only gives good results are used to draw the curve for experimental results. In this section, all value utilized to draw the curve, the value measured from the experiments after the impact events are given in following table. Where, E_i, E_a, t_c, δ_{max}, and F_{max} represent the impact energy, absorbed energy and contact time, maximum value of deflection and maximum value of contact force, respectively.

Table A.1 Measured all value for E_i, E_a, t_c, δ_{max} and F_{max} due to size of delamination at the energy level of 5 J

E_i (J)	Material Properties	Experiment Number	E_a (J)	t_c (ms)	δ_{max}(mm)	F_{max} (N)
5	C0d0	1	2,973	8,000	4,097	2581,410
		2	2,950	7,752	3,888	2588,969
		3	2,869	7,916	3,921	2551,174
		4	2,959	8,048	4,018	2523,772
		5	2,888	7,980	3,949	2563,457
		Mean	**2,928**	**7,939**	**3,975**	**2561,756**
		Sd.	**0,046**	**0,115**	**0,083**	**25,906**
	C13d2	1	2,983	8,084	4,027	2485,977
		2	2,905	8,140	4,035	2525,662
		3	2,992	7,976	3,994	2534,166
		4	3,017	7,948	3,971	2519,993
		5	2,971	8,032	4,016	2521,882
		Mean	**2,974**	**8,036**	**4,008**	**2517,536**
		Sd.	**0,042**	**0,078**	**0,026**	**18,463**
	C20d2	1	2,977	8,060	4,021	2524,717
		2	3,030	7,928	3,984	2524,717
		3	3,024	7,952	3,979	2516,213
		4	3,021	8,256	4,141	2507,709
		5	2,921	8,112	4,023	2520,937
		Mean	**2,994**	**8,062**	**4,030**	**2518,859**
		Sd.	**0,046**	**0,132**	**0,066**	**7,146**
	C26d2	1	2,981	8,024	4,002	2561,567
		2	3,004	7,964	3,951	2538,890
		3	3,135	7,952	4,025	2542,670
		4	3,008	8,052	4,044	2562,512
		5	3,009	7,964	4,003	2538,890
		Mean	**3,027**	**7,991**	**4,005**	**2548,906**
		Sd.	**0,061**	**0,044**	**0,035**	**12,093**

Table A.2 Measured all value for E_i, E_a, t_c, δ_{max} and F_{max} due to size of delamination at the energy level of 10 J

E_i (J)	Material Properties	Experiment Number	E_a (J)	t_c (ms)	δ_{max}(mm)	F_{max} (N)
10	C0d0	1	8,917	7,275	5,744	3994,004
		2	5,808	7,724	5,236	3800,304
		3	5,854	7,624	5,168	3814,477
		4	5,862	7,576	5,114	3848,493
		5	5,897	7,604	5,134	3829,595
		Mean	**6,467**	**7,561**	**5,279**	**3857,374**
		Sd.	**1,370**	**0,169**	**0,264**	**78,447**
	C13d2	1	9,120	7,288	5,793	3998,728
		2	8,946	7,700	6,130	3811,642
		3	9,003	7,663	6,048	3818,256
		4	8,597	7,713	5,886	3847,548
		5	8,606	7,563	5,755	3829,595
		Mean	**8,854**	**7,585**	**5,923**	**3861,154**
		Sd.	**0,239**	**0,176**	**0,162**	**78,102**
	C20d2	1	8,962	7,300	5,788	4026,130
		2	8,554	7,775	5,953	3823,926
		3	8,466	7,700	5,855	3822,036
		4	8,759	7,675	5,801	3817,312
		5	8,942	7,588	6,080	3790,855
		Mean	**8,737**	**7,608**	**5,895**	**3856,052**
		Sd.	**0,223**	**0,184**	**0,122**	**96,004**
	C26d2	1	8,304	7,413	5,583	4032,744
		2	8,533	7,825	6,100	3876,839
		3	8,866	7,663	6,125	3761,564
		4	8,734	7,788	6,099	3805,028
		5	8,349	7,675	5,860	3863,611
		Mean	**8,557**	**7,673**	**5,954**	**3867,957**
		Sd.	**0,242**	**0,161**	**0,233**	**103,117**

Table A.3 Measured all value for E_i, E_a, t_c, δ_{max} and F_{max} due to size of delamination at the energy level of 20 J

E_i (J)	Material Properties	Experiment Number	E_a (J)	t_c (ms)	δ_{max}(mm)	F_{max} (N)
20	C0d0	1	12,6812	7,684	7,2042	5811,006
		2	12,9823	7,788	7,2337	5636,204
		3	13,3337	7,752	7,2028	5645,653
		4	11,6438	7,484	7,0857	6119,037
		5	12,0608	7,448	7,0614	6119,037
		Mean	**12,540**	**7,631**	**7,158**	**5866,187**
		Sd.	**0,685**	**0,156**	**0,078**	**241,060**
	C13d2	1	11,3618	7,356	7,0652	6121,872
		2	11,5449	7,416	7,0952	6129,431
		3	12,2915	7,496	7,0976	6083,132
		4	11,4511	7,4	7,0978	6141,714
		5	11,4793	7,392	7,0907	6116,202
		Mean	**11,626**	**7,412**	**7,089**	**6118,470**
		Sd.	**0,378**	**0,052**	**0,014**	**21,943**
	C20d2	1	12,7596	7,664	7,2247	5948,014
		2	12,2237	7,528	7,2057	5955,573
		3	11,5823	7,408	7,0905	6085,021
		4	12,8319	7,632	7,2114	5823,29
		5	11,8752	7,428	7,169	6023,604
		Mean	**12,25454**	**7,532**	**7,18026**	**5967,1**
		Sd.	**0,544**	**0,116**	**0,054**	**97,822**
	C26d2	1	11,8957	7,46	7,167	5994,313
		2	11,7751	7,464	7,1461	6124,706
		3	12,2607	7,568	7,1899	6028,329
		4	12,635	7,732	7,383	5875,258
		5	12,1044	7,604	7,1789	5959,352
		Mean	**12,13418**	**7,5656**	**7,21298**	**5996,392**
		Sd.	**0,337**	**0,113**	**0,096**	**91,562**

Table A.4 Measured all value for E_i, E_a, t_c, δ_{max} and F_{max} due to location of delamination at the energy level of 20 J

E_i (J)	Material Properties	Experiment Number	E_a (J)	t_c (ms)	δ_{max}(mm)	F_{max} (N)
20	C13d4	1	11,9701	7,256	6,6998	5934,786
		2	11,4808	7,332	6,6789	5914,943
		3	11,0945	7,2	6,6875	5964,077
		4	11,7617	7,24	6,7144	5839,353
		5	11,9481	7,344	6,7178	5749,589
		Mean	**11,65104**	**7,2744**	**6,69968**	**5880,55**
		Sd.	**0,368**	**0,062**	**0,017**	**86,529**
	C13d6	1	11,3419	7,256	6,6632	5880,928
		2	10,7539	7,164	6,5622	6130,376
		3	11,6214	7,14	6,6014	6036,833
		4	11,9847	7,28	6,7211	5725,023
		5	10,7	7,064	6,599	6115,258
		Mean	**11,28038**	**7,1808**	**6,62938**	**5977,683**
		Sd.	**0,555**	**0,088**	**0,063**	**172,438**
	C13d2/4	1	10,2838	7,264	6,6921	6094,47
		2	10,0914	7,184	6,6319	6193,683
		3	10,0422	7,136	6,6022	6217,305
		4	10,3364	7,264	6,7185	6098,25
		5	10,4499	7,252	6,7004	6054,785
		Mean	**10,24074**	**7,22**	**6,66902**	**6131,698**
		Sd.	**0,171**	**0,058**	**0,050**	**69,984**
	C13d2/4/6	1	9,8833	7,148	6,6978	6255,1
		2	10,1476	7,128	6,7781	6035,888
		3	10,3153	7,08	6,756	6025,494
		4	12,0519	7,26	6,8081	5516,204
		5	9,9481	7,128	6,7329	6116,202
		Mean	**10,46924**	**7,1488**	**6,75458**	**5989,778**
		Sd.	**0,901**	**0,067**	**0,042**	**280,202**

Table A.5 Measured all value for E_i, E_a, t_c, δ_{max} and F_{max} due to size of delamination at the energy level of 30 J

E_i (J)	Material Properties	Experiment Number	E_a (J)	t_c (ms)	δ_{max}(mm)	F_{max} (N)
30	C0d0	1	21,7058	7,5625	8,5093	7012,893
		2	22,471	7,82	8,7372	6999,664
		3	19,8395	7,596	8,5066	7251,002
		4	21,5314	7,684	8,5973	7069,585
		5	21,8009	7,712	8,5119	7304,86
		Mean	**21,46972**	**7,6749**	**8,57246**	**7127,601**
		Sd.	**0,978**	**0,102**	**0,100**	**141,014**
	C13d2	1	21,5613	7,525	8,3385	7317,144
		2	22,0871	7,4125	8,5187	6754,941
		3	21,0682	7,5375	8,4511	7196,199
		4	20,4854	7,525	8,3146	7692,261
		5	21,0822	7,5125	8,4554	7491,001
		Mean	**21,25684**	**7,5025**	**8,41566**	**7290,309**
		Sd.	**0,601**	**0,051**	**0,086**	**352,859**
	C20d2	1	21,1812	7,625	8,6041	7062,026
		2	20,6892	7,6125	8,3759	7022,341
		3	21,1031	7,75	8,6057	6709,586
		4	21,7596	7,575	8,4375	7176,357
		5	21,2517	7,6	8,6641	6977,932
		Mean	**21,19696**	**7,6325**	**8,53746**	**6989,649**
		Sd.	**0,383**	**0,068**	**0,124**	**173,017**
	C26d2	1	22,455	7,625	8,6319	7000,609
		2	21,5237	7,6375	8,7172	6741,712
		3	22,7233	7,775	8,5885	7061,081
		4	22,2847	7,5875	8,6138	7123,444
		5	22,1295	7,7	8,558	6901,397
		Mean	**22,22324**	**7,665**	**8,62188**	**6965,649**
		Sd.	**0,449**	**0,074**	**0,060**	**149,587**

Table A.6 Measured all value for E_i, E_a, t_c, δ_{max} and F_{max} due to location of delamination at the energy level of 30 J

E_i (J)	Material Properties	Experiment Number	E_a (J)	t_c (ms)	δ_{max}(mm)	F_{max} (N)
30	C13d4	1	18,6365	7,46	8,078	7243,443
		2	19,5443	7,1	7,9837	6658,563
		3	18,1824	7,492	8,045	7028,956
		4	18,7594	7,604	8,1288	6731,319
		5	19,1901	7,16	8,0307	6667,067
		Mean	**18,86254**	**7,3632**	**8,05324**	**6865,869**
		Sd.	**0,524**	**0,221**	**0,054**	**259,693**
	C13d6	1	19,7078	7,548	7,9806	7026,121
		2	18,6587	7,572	8,079	6734,153
		3	19,7791	7,672	8,1889	7004,389
		4	19,1506	7,468	8,0986	7014,782
		5	21,0737	7,596	8,0755	6870,216
		Mean	**19,67398**	**7,5712**	**8,08452**	**6929,932**
		Sd.	**0,905**	**0,074**	**0,074**	**126,383**
	C13d2/4	1	18,1889	7,496	8,0499	7300,136
		2	18,9972	7,54	8,0043	7227,38
		3	19,1547	7,504	7,9885	7196,199
		4	19,3569	7,588	8,0409	7490,057
		5	18,7334	7,48	8,043	7199,979
		Mean	**18,88622**	**7,5216**	**8,02532**	**7282,75**
		Sd.	**0,452**	**0,043**	**0,027**	**123,173**
	C13d2/4/6	1	17,5025	7,36	8,0482	7491,002
		2	18,4552	7,52	8,0939	7506,12
		3	18,8243	7,388	7,9663	7708,324
		4	19,8564	7,536	8,0854	7696,985
		5	18,6385	7,392	8,0721	7289,742
		Mean	**18,65538**	**7,4392**	**8,05318**	**7538,434**
		Sd.	**0,843**	**0,082**	**0,052**	**172,585**

Table A.7 Measured all value for E_i, E_a, t_c, δ_{max} and F_{max} due to size of delamination at the energy level of 40 J

E_i (J)	Material Properties	Experiment Number	E_a (J)	t_c (ms)	δ_{max}(mm)	F_{max} (N)
40	C0d0	1	34,6078	8,0875	9,9505	7312,419
		2	34,5968	8,4125	9,9765	7621,395
		3	33,1521	8,28	10,0525	7260,92
		4	34,7808	8,828	10,1656	7151,787
		5	34,1534	8,62	10,1845	7336,038
		Mean	**34,25818**	**8,4456**	**10,06592**	**7336,512**
		Sd.	**0,660**	**0,289**	**0,107**	**174,339**
	C13d2	1	33,0886	7,6625	9,6402	7636,513
		2	34,235	8,3875	10,034	7350,214
		3	33,2214	7,775	9,7134	7263,286
		4	34,1591	8,175	9,8291	7397,458
		5	32,9502	8,0625	9,7506	7203,758
		Mean	**33,53086**	**8,0125**	**9,79346**	**7370,246**
		Sd.	**0,616**	**0,295**	**0,151**	**166,732**
	C20d2	1	34,2114	7,9625	9,93	7493,836
		2	35,4032	8,6375	10,3443	7019,507
		3	33,0138	8,2	10,025	6936,357
		4	35,2405	8,6375	10,3613	6927,854
		5	35,233	8,6375	10,3603	6950,531
		Mean	**34,62038**	**8,415**	**10,20418**	**7065,617**
		Sd.	**1,015**	**0,316**	**0,210**	**242,090**
	C26d2	1	34,7212	8,5375	10,2059	7342,655
		2	33,8138	8,0875	10,0436	7698,875
		3	32,8	7,9	9,8767	7703,599
		4	32,8034	8,0875	9,9548	7663,914
		5	34,0613	7,9875	9,8642	7700,765
		Mean	**33,63994**	**8,12**	**9,98904**	**7621,962**
		Sd.	**0,834**	**0,246**	**0,141**	**156,973**

Table A.8 Measured all value for E_i, E_a, t_c, δ_{max} and F_{max} due to location of delamination at the energy level of 40 J

E_i (J)	Material Properties	Experiment Number	E_a (J)	t_c (ms)	δ_{max}(mm)	F_{max} (N)
40	C13d4	1	33,6868	7,888	9,448	7044,071
		2	32,8073	7,484	9,4384	7228,322
		3	34,8564	7,508	9,3288	6954,78
		4	34,3127	7,968	9,8267	6797,457
		5	32,1871	7,672	9,4168	7197,141
		Mean	**33,57006**	**7,704**	**9,49174**	**7044,354**
		Sd.	**1,086**	**0,219**	**0,193**	**177,602**
	C13d6	1	33,1123	7,744	9,448	7411,156
		2	34,38	7,864	9,3615	7143,283
		3	31,1895	7,472	9,1446	7881,706
		4	34,8854	7,884	9,7381	6594,781
		5	32,4299	7,388	9,3113	7535,88
		Mean	**33,19942**	**7,6704**	**9,4007**	**7313,361**
		Sd.	**1,490**	**0,228**	**0,219**	**481,502**
	C13d2/4	1	32,3707	7,9	9,384	7776,824
		2	32,1917	7,868	9,4036	7477,77
		3	31,8866	7,328	9,2182	6991,63
		4	33,3707	7,944	9,5362	6956,197
		5	31,3497	7,22	9,1101	7565,644
		Mean	**32,23388**	**7,652**	**9,33042**	**7353,613**
		Sd.	**0,744**	**0,348**	**0,167**	**363,473**
	C13d2/4/6	1	32,9695	7,376	9,2212	7433,833
		2	31,6879	7,096	9,0085	7690,368
		3	32,9905	7,516	9,5028	6906,591
		4	33,7419	7,568	9,4437	7898,713
		5	31,9799	7,524	9,516	7321,865
		Mean	**32,67394**	**7,416**	**9,33844**	**7450,274**
		Sd.	**0,834**	**0,193**	**0,219**	**377,854**

Table A.9 Measured all value for E_i, E_a, t_c, δ_{max} and F_{max} due to size of delamination at the energy level of 50 J

E_i (J)	Material Properties	Experiment Number	E_a (J)	t_c (ms)	δ_{max}(mm)	F_{max} (N)
50	C0d0	1	48,011	9,8875	12,3477	7017,617
		2	47,1855	9,475	12,0127	7547,694
		3	47,9234	11,504	12,8615	7317,613
		4	47,7732	11,12	12,7725	7073,834
		5	50,3599	11,364	17,9642	6862,654
		Mean	**48,2506**	**10,6701**	**13,59172**	**7163,882**
		Sd.	**1,222**	**0,925**	**2,468**	**269,808**
	C13d2	1	47,0095	9,5375	11,5609	7674,308
		2	47,5563	9,9375	12,3105	7107,381
		3	46,1083	9,55	11,8942	7464,545
		4	46,8896	9,65	11,7446	7716,828
		5	46,8142	8,9625	11,5219	7648,796
		Mean	**46,87558**	**9,5275**	**11,80642**	**7522,371**
		Sd.	**0,518**	**0,355**	**0,319**	**251,218**
	C20d2	1	46,7241	9,4125	11,5141	7726,276
		2	45,8558	9,325	11,7308	7587,379
		3	47,2519	10,1625	12,2412	7360,608
		4	47,1575	9,5875	11,8931	7557,143
		5	46,6659	9,275	11,8279	7651,631
		Mean	**46,73104**	**9,5525**	**11,84142**	**7576,607**
		Sd.	**0,553**	**0,361**	**0,266**	**137,095**
	C26d2	1	45,8416	8,775	11,3376	7571,316
		2	44,5293	8,725	11,4298	7645,962
		3	45,2319	8,9375	11,6978	7710,213
		4	44,5637	8,9875	11,5523	7621,395
		5	44,8508	8,875	11,6293	7719,662
		Mean	**45,00346**	**8,86**	**11,52936**	**7653,71**
		Sd.	**0,547**	**0,109**	**0,146**	**62,120**

Table A.10 Measured all value for E_i, E_a, t_c, δ_{max} and F_{max} due to location of delamination at the energy level of 50 J

E_i (J)	Material Properties	Experiment Number	E_a (J)	t_c (ms)	δ_{max}(mm)	F_{max} (N)
50	C13d4	1	45,2203	9,504	11,3303	7816,509
		2	44,8022	8,92	11,2491	7173,047
		3	48,3994	10,668	11,8842	7310,526
		4	45,1661	9,072	11,1398	7754,147
		5	45,6051	9,36	11,5372	7653,517
		Mean	**45,83862**	**9,5048**	**11,42812**	**7541,549**
		Sd.	**1,460**	**0,690**	**0,294**	**283,947**
	C13d6	1	44,1212	8,392	11,0117	7851,942
		2	50,0023	9,564	14,2051	7518,872
		3	45,9451	9,388	11,611	7888,792
		4	44,4189	9,32	11,1474	7483,439
		5	47,6499	9,72	11,6964	7694,62
		Mean	**46,42748**	**9,2768**	**11,93432**	**7687,533**
		Sd.	**2,442**	**0,519**	**1,303**	**185,531**
	C13d2/4	1	45,7	9,728	11,5549	7856,194
		2	43,938	8,9	10,9049	8250,208
		3	44,0073	9,104	10,8161	8528,003
		4	44,7267	9,484	11,3322	7878,871
		5	46,2881	9,368	11,1732	8329,578
		Mean	**44,93202**	**9,3168**	**11,15626**	**8168,571**
		Sd.	**1,039**	**0,324**	**0,304**	**292,953**
	C13d2/4/6	1	47,5634	8,36	11,5929	7823,596
		2	44,728	8,3	10,7399	8462,806
		3	46,2224	8,784	11,1341	8376,35
		4	45,3668	8,904	11,2147	8095,721
		5	46,6081	8,94	11,5134	7691,785
		Mean	**46,09774**	**8,6576**	**11,239**	**8090,051**
		Sd.	**1,099**	**0,305**	**0,340**	**335,619**